
This is an electronic reprint of the original article.
This reprint may differ from the original in pagination and typographic detail.

Holmberg, Nico; Laasonen, Kari

Efficient Constrained Density Functional Theory Implementation for Simulation of Condensed Phase Electron Transfer Reactions

Published in:
Journal of Chemical Theory and Computation

DOI:
[10.1021/acs.jctc.6b01085](https://doi.org/10.1021/acs.jctc.6b01085)

Published: 23/12/2016

Document Version
Peer-reviewed accepted author manuscript, also known as Final accepted manuscript or Post-print

Published under the following license:
Unspecified

Please cite the original version:
Holmberg, N., & Laasonen, K. (2016). Efficient Constrained Density Functional Theory Implementation for Simulation of Condensed Phase Electron Transfer Reactions. *Journal of Chemical Theory and Computation*, 13(2), 587-601. <https://doi.org/10.1021/acs.jctc.6b01085>

This material is protected by copyright and other intellectual property rights, and duplication or sale of all or part of any of the repository collections is not permitted, except that material may be duplicated by you for your research use or educational purposes in electronic or print form. You must obtain permission for any other use. Electronic or print copies may not be offered, whether for sale or otherwise to anyone who is not an authorised user.

To access the final edited and published work see <http://pubs.acs.org/doi/10.1021/acs.jctc.6b01085>

J. Chem. Theory Comput., 2017, x (xx), pp xx1-xx16, DOI: 10.1021/acs.jctc.6b01085

Efficient Constrained Density Functional Theory Implementation for Simulation of Condensed Phase Electron Transfer Reactions

Nico Holmberg and Kari Laasonen*

*COMP Centre of Excellence in Computational Nanoscience, Department of Chemistry,
Aalto University, P.O. Box 16100, FI-00076 Aalto, Finland*

E-mail: kari.laasonen@aalto.fi

Abstract

Constrained density functional theory (CDFT) is a versatile tool for probing the kinetics of electron transfer (ET) reactions. In this work, we present a well-scaling parallel CDFT implementation relying on a mixed basis set of Gaussian functions and planewaves, which has been specifically tailored to investigate condensed phase ET reactions using an explicit, quantum chemical representation of the solvent. The accuracy of our implementation is validated against previous theoretical results for predicting electronic couplings and charge transfer energies. Subsequently, we demonstrate the efficiency of our method by studying the intramolecular ET reaction of an organic mixed valence compound in water using a CDFT based molecular dynamics simulation.

Keywords

Marcus theory, solvent reorganization energy, electronic coupling, molecular dynamics, charge constraint, electron transfer kinetics

Efficient Constrained Density Functional Theory Implementation for Simulation of Condensed Phase Electron Transfer Reactions

Nico Holmberg and Kari Laasonen*

*COMP Centre of Excellence in Computational Nanoscience, Department of Chemistry,
Aalto University, P.O. Box 16100, FI-00076 Aalto, Finland*

E-mail: kari.laasonen@aalto.fi

Abstract

Constrained density functional theory (CDFT) is a versatile tool for probing the kinetics of electron transfer (ET) reactions. In this work, we present a well-scaling parallel CDFT implementation relying on a mixed basis set of Gaussian functions and plane waves, which has been specifically tailored to investigate condensed phase ET reactions using an explicit, quantum chemical representation of the solvent. The accuracy of our implementation is validated against previous theoretical results for predicting electronic couplings and charge transfer energies. Subsequently, we demonstrate the efficiency of our method by studying the intramolecular ET reaction of an organic mixed valence compound in water using a CDFT based molecular dynamics simulation.

Keywords

Marcus theory, solvent reorganization energy, electronic coupling, molecular dynamics, charge constraint, electron transfer kinetics

1 Introduction

Electron transfer (ET) reactions are ubiquitous in nature, serving a vital function in mitochondrial aerobic respiration¹⁻³ and a myriad of other redox processes in proteins.^{4,5} Atomistic modeling of electron transfer kinetics is frequently founded on the linear response theory pioneered by Marcus,⁶ which has been extended to cover a wide range of phenomena^{7,8} including ET processes at electrodes,^{9,10} proton-coupled ET,¹¹ and reactions with large solvation changes.¹² By assuming that the underlying probability distributions describing the electron transfer initial (*a*) and final (*b*) diabatic states are Gaussians with equal curvature, the Marcus rate constant for a homogeneous diabatic ET reaction is given by¹³

$$k_{\text{ET}} = \frac{2\pi}{\hbar} \frac{\langle |H_{ab}|^2 \rangle_T}{\sqrt{4\pi k_{\text{B}} T \lambda}} \exp \left[-\frac{(\lambda + \Delta A)^2}{4k_{\text{B}} T \lambda} \right] \quad (1)$$

where $|H_{ab}|$ is the electronic coupling between ET states, defined rigorously in terms of the *N*-electron wavefunctions Ψ_i and the electronic Hamiltonian \mathcal{H} as $|H_{ab}| = |\langle \Psi_a | \mathcal{H} | \Psi_b \rangle|$, λ is the reorganization free energy, ΔA the reaction Helmholtz free energy, and thermal averaging over nuclear configurations is indicated by the canonical average $\langle \cdot \rangle_T$. The equation further allows the activation free energy to be identified as $\Delta A^\ddagger = (\lambda + \Delta A)^2 / (4\lambda)$. Explicitly, λ describes the free energy required to change the equilibrium configuration of diabatic state *a* into the equilibrium configuration of diabatic state *b* while remaining on the parabolic free energy curve of *a*, and is equivalent to the reverse relation with states permuted within the linear response regime. Blumberger⁵ has recently reviewed the derivation and inherent assumptions of the Marcus rate equation (1) and they will consequently not be covered in this presentation.

A variety of theoretical methods are available for modeling the ET parameters in Equation (1). For $|H_{ab}|$, these include the generalized Mulliken Hush (GMH) method,^{14,15} localization and block diagonalization methods,¹⁵⁻²¹ and constrained density functional theory (CDFT).²²⁻²⁴ A more exhaustive list of methods can be found in literature^{5,25-33} and we

refer the interested readers to these and references therein for a comparison of the different approaches. In this context, however, we wish to highlight that CDFT is a particularly appealing alternative to compute $|H_{ab}|$ since it combines the computational efficiency of traditional DFT with often great accuracy,^{22,23,30} except in pathological cases where fractional charge is transferred.³⁴ The modest cost of CDFT also facilitates studying ET processes under dynamical conditions using molecular dynamics (MD) coupled with an all atom description of the solvent. Therefore, a single set of simulations performed at a consistent level of theory can be used to quantify all the parameters ($|H_{ab}|$, λ , ΔA) appearing in the Marcus rate equation (1), which is clearly impossible, for instance, with wavefunction based methods. This capability is particularly important to investigate the validity of the Condon approximation and solvation effects. Although CDFT has occasionally been criticized for a lack of predictive power since the diabatic states must be predefined, it should be noted that unconstrained DFT in itself usually struggles with generating the necessary charge localized diabatic states due to self-interaction error,³⁵ although the usage of hybrid or other high level exchange-correlation functionals might alleviate the issue in some cases.³⁶

While previous applications of CDFT include examples where condensed phase ET reactions were studied with MD – e.g. self-exchange between ruthenium cations^{37,38} or intramolecular ET within a donor-acceptor dyad,³⁹ to name just a couple of examples – in most of these studies only one of the participating ET states (a or b) has been explicitly included in the CDFT MD simulation, whereas the necessary quantities involving both states have been computed as a series of postproduction single point calculations. A notable exception to this is the seminal CDFT implementation due to de la Lande and coworkers,^{24,40} where both ET states are solved in serial during MD. This has facilitated for example the quantification of dynamical quantum effects in the ET within cryptochromes via hybrid CDFT/molecular mechanics (MM) simulations.⁴¹ A similar strategy has, to our knowledge, thus far not been applied to MD simulations at the full CDFT level. We speculate that such calculations have not been attempted with current CDFT capable software^{22–24,37,40,42–47}

mainly due to the high associated computational cost, which is ultimately governed by the underlying DFT implementation, in particular the choice of basis set and electronic structure solver. A computational framework that is, in this respect, ideally suited for such large scale condensed phase MD simulations is the mixture of the orbital transformation⁴⁸ solver with a dual basis set of Gaussians and planewaves,⁴⁹ as implemented in the CP2K^{50,51} code, which has routinely been applied to systems containing hundreds of atoms, see for example Refs. 52–54.

In this work, we will present a CDFT algorithm that exploits this framework and enables the concurrent simulation of both ET states using constrained molecular dynamics. To this end, we will first summarize the connection between CDFT and Marcus theory, and subsequently describe the necessary ingredients of our algorithm in Section 2. It will also be discussed when and why it is advantageous to treat both ET states in parallel. After a brief description of the computational methods in Section 3, we will validate our implementation against ab initio wavefunction calculations for predicting electronic couplings for various gas phase systems, as well as against another CDFT implementation for evaluating charge transfer energies of noncovalent complexes in Sections 4.1-4.2. Thereafter, the main results of this work will be presented in Section 4.3 where the intramolecular ET reaction of an organic mixed valence anion is investigated using a condensed phase CDFT MD simulation. These results are discussed in view of experimental measurements and previous theoretical work. Finally, a brief analysis regarding the influence of computational parameters on the quality of CDFT results is given in Section 4.4. Additional technical details behind the current CDFT implementation are presented in Appendices A-B.

2 Theory

2.1 Constrained Density Functional Theory Applied to Electron Transfer Reactions

Building upon the earlier work of Dederichs and coworkers,⁵⁵ Wu and Van Voorhis^{22,42,56} introduced a fully general CDFT energy functional which supports arbitrary constraints and is the current basis of all CDFT implementations. Here, only a minimal summary of the theory behind CDFT will be given as it pertains to this work. More extensive discussions can be found in the original research papers^{22,42,56} or e.g. in the comprehensive review article of Ref. 30. Assuming a single, spin independent constraint, the constrained electronic state of a system is sought through Lagrangian optimization of an energy functional, E_{CDFT} , where the standard Kohn-Sham energy functional, E_{KS} , is augmented with an additional constraint potential

$$E_{\text{CDFT}}[\rho, \xi] = \max_{\xi} \min_{\rho} \left\{ E_{\text{KS}}[\rho] + \xi \left(\int w(\mathbf{r})\rho(\mathbf{r})d\mathbf{r} - N_c \right) \right\} \quad (2)$$

In this expression, $w(\mathbf{r})$ is a weight function that imposes the wanted constraint conditions, ξ is the Lagrange multiplier associated with the constraint, and N_c is the target value of the constraint. Depending on the functional form of the constraint, it is possible to constraint either absolute charges on atoms or charge differences between an acceptor and a donor. In both cases, the constraint can also be defined relative to a noninteracting reference state^{57,58}

$$\tilde{N}_c = \int w(\mathbf{r})[\tilde{\rho}_A(\mathbf{r}) + \tilde{\rho}_B(\mathbf{r})]d\mathbf{r} \quad (3)$$

where $\tilde{\rho}_i$ is the unconstrained electron density of the isolated fragment i , and to avoid confusion \tilde{N}_c is used to denote the fragment based constraint target value. The stationary point of E_{CDFT} is in practice located using a two tiered self-consistent field (SCF) approach

with alternating minimizations along ρ and maximizations along ξ .⁵⁶ For molecular dynamics simulations, the force on atom i , \mathbf{F}_i , at position \mathbf{R}_i must naturally be supplemented with a term $\mathbf{F}_{c,i}$ arising from the constraint

$$\mathbf{F}_{c,i} = -\xi \int \frac{\partial w(\mathbf{r})}{\partial \mathbf{R}_i} \rho(\mathbf{r}) d\mathbf{r} \quad (4)$$

Any population analysis method can in principle be used to define $w(\mathbf{r})$, although as a general rule of thumb real space based partition schemes, such as the Hirshfeld⁵⁹ and Becke⁶⁰ methods, have been shown to perform better than, for instance, orbital based schemes.³⁰ We have based our CDFT implementation on the Becke weight function and a detailed description on the efficient construction of the constraint will be given in Sections 2.2-2.3.

A connection between CDFT and Marcus theory can be established by first recalling that two states, the initial a and final b states, are sufficient to characterize the kinetics of an ET reaction. CDFT treatment of these states is straightforward as they only differ in the way the constraint is defined (different values of N_c). These calculations produce localized diabatic states with characteristic Kohn-Sham wavefunctions, Φ_I , that are in general mutually nonorthogonal but can nonetheless be employed to define a diabatic coupling $|H_{AB}|$ ³⁰

$$|H_{AB}| \approx \langle \Phi_A | \mathcal{H}_{KS} | \Phi_B \rangle = \frac{E_A + E_B}{2} S_{AB} - \frac{\xi_A + \xi_B}{2} \langle \Phi_A | w(\mathbf{r}) | \Phi_B \rangle \quad (5)$$

where E_I is the CDFT energy of diabatic state I, S_{AB} is the overlap between states, and capital subscripts have been used to distinguish the states from their orthogonal counterparts. An orthogonalization procedure is then followed to arrive at a CDFT approximation of the coupling $|H_{ab}|$ which appears in the Marcus rate equation (1).^{22,23} In order to estimate the required free energy quantities λ and ΔA , Warshel's⁶¹ microscopic interpretation of Marcus theory is adopted. Within this formalism, the quantity describing the ET process is the vertical energy gap, ΔE , which is evaluated as the energy difference of the two constrained ET states at fixed atomic configuration \mathbf{R}^N

$$\Delta E(\mathbf{R}^N) = E_B(\mathbf{R}^N) - E_A(\mathbf{R}^N) \quad (6)$$

The reorganization free energy, λ , and the reaction free energy, ΔA , can be obtained by sampling ΔE during constrained molecular dynamics simulations. Assuming that the system is in the linear response limit and the fluctuations of ΔE obey Gaussian statistics, the key assumptions of Marcus theory (see e.g. Ref. 12), the relevant identities are

$$\lambda = \frac{\langle \Delta E_A \rangle_T - \langle \Delta E_B \rangle_T}{2} \quad (7)$$

$$\Delta A = \frac{\langle \Delta E_A \rangle_T + \langle \Delta E_B \rangle_T}{2} \quad (8)$$

where $\langle \Delta E_I \rangle_T$ denotes the canonical average of ΔE obtained from a CDFT MD simulation where the nuclei have been propagated on the potential energy surface of state I.

2.2 Efficient Construction of the Becke Constraint

Construction of the Becke weight function essentially involves dividing the system into Voronoi polyhedra that are smoothed to avoid discontinuities.⁶⁰ The construction of these Becke cells, however, scales unfavorably with system size, which is a major drawback for condensed phase simulations. To elaborate this matter further, let $\mathcal{W} = \mathcal{A} \cup \mathcal{D}$ denote the set of constraint atoms, where acceptor and donor atoms are collected in the disjoint sets \mathcal{A} and \mathcal{D} , respectively. Defining \mathcal{N} further as the set of all atoms within the system, the Becke⁶⁰ real space weight function (BW) can then be expressed as

$$w(\mathbf{r}) = \sum_{i \in \mathcal{W}} c_i w_i(\mathbf{r}) = \frac{\sum_{i \in \mathcal{W}} c_i P_i(\mathbf{r})}{\sum_{n \in \mathcal{N}} P_n(\mathbf{r})}, \quad c_i = \begin{cases} +1, & \text{if } i \in \mathcal{A} \\ -1, & \text{if } i \in \mathcal{D} \end{cases} \quad (9)$$

where $P_i(\mathbf{r}) = \prod_{\substack{j \in \mathcal{N} \\ j \neq i}} s(\mu_{ij})$ is the so-called cell function, constructed from the products of

smoothed step functions (high order polynomials), s , and where the coefficient c_i changes sign based on whether the atom is an electron acceptor or donor. Here, the argument of the step function, μ_{ij} , is the hyperboloidal coordinate function defined for each atom pair i, j positioned at $\mathbf{R}_i, \mathbf{R}_j$ as

$$\mu_{ij}(\mathbf{r}) = \frac{|\mathbf{R}_i - \mathbf{r}| - |\mathbf{R}_j - \mathbf{r}|}{|\mathbf{R}_i - \mathbf{R}_j|} = \frac{r_i - r_j}{R_{ij}} \quad (10)$$

The density partitioning defined thus far treats every element equally, which leads to unphysical atomic charges even in the simplest molecules such as water, predicting a negative charge on hydrogen atoms and a positive charge on oxygen. In his original work, Becke⁶⁰ already acknowledged this issue and suggested shifting the cell boundaries off center with the transformation $\nu_{ij} = \mu_{ij} + a_{ij}(1 - \mu_{ij}^2)$, where a_{ij} is an atom pair specific parameter depending on the radii of the atoms. There is naturally no unique way to define atomic radii and in our implementation the choice is left to the user. Regardless, this transformation is at the core of our method as it facilitates introducing a heteronuclear density partitioning (BW+A) by simply substituting μ_{ij} for ν_{ij} in Equation (9), leading to an improved description of partial charges and e.g. $|H_{ab}|$ values (see Section 4). Now, the necessary gradient to compute atomic forces arising from the constraint (Equation (4)) is given by

$$\frac{\partial w(\mathbf{r})}{\partial \mathbf{R}_i} = \frac{1}{\sum_{n \in \mathcal{N}} P_n(\mathbf{r})} \left(c_i \frac{\partial P_i(\mathbf{r})}{\partial \mathbf{R}_i} + \sum_{\substack{j \in \mathcal{W} \\ j \neq i}} c_j \frac{\partial P_j(\mathbf{r})}{\partial \mathbf{R}_i} \right) - \frac{\sum_{i \in \mathcal{W}} c_i P_i(\mathbf{r})}{\left(\sum_{n \in \mathcal{N}} P_n(\mathbf{r}) \right)^2} \sum_{n \in \mathcal{N}} \frac{\partial P_n(\mathbf{r})}{\partial \mathbf{R}_i} \quad (11)$$

where the first term on the r.h.s. vanishes if atom i is not a constraint atom. All the necessary identities required to implement the heteronuclear Becke method with forces have been derived in Appendix A.

Examination of Equations (9)-(11) reveals the origin of poor scaling of the Becke method with system size. Specifically, as the method requires iterating through every atom pair

ij permutation at every real space point \mathbf{r} , a large fraction of computational time during electronic structure optimization will actually be spent in building the constraint. This problem becomes more pronounced in condensed phase simulations, and a direct CDFT implementation based on the above equations is prohibitively costly for MD simulations. Fortunately, the computational cost of the Becke method can be considerably decreased by meticulously analyzing the properties of the weight function. First, observe that the weight function and its gradients are only functions of atomic positions \mathbf{R}_i , and in particular do not depend on $\rho(\mathbf{r})$. Accordingly, both terms can be calculated simultaneously and stored in memory prior to starting the SCF optimization of the electronic structure. On each SCF iteration, it is then straightforward to enforce the constraint by evaluating the integrals of Equations (2) and (4).

Another key strategy for improving the performance of the Becke algorithm is to confine the density partitioning to a smaller subspace, which in fact can be implemented without any loss of accuracy. In order to establish this property, consider an arbitrary grid point \mathbf{r} within the periodic supercell. Only a handful of atoms are located close to this grid point, say within a few Å, even in the condensed phase. The contribution of any other atom to the weight function $w(\mathbf{r})$ will quickly tend to zero the farther the atom resides from the grid point, because the closest atoms dominate the expression by virtue of using smoothed step functions to define $w(\mathbf{r})$ (for further elaboration, see also Appendix A). To take advantage of this observation, an element specific cutoff radius is introduced to automatically discard those atoms i that reside beyond a cutoff radius away from the current grid point and nothing is calculated for the atom pairs ij . However, the reverse pairs ji still need to be calculated, assuming atom j is within the cutoff radius.

Building upon the previous idea, a significantly higher reduction in computational cost can be achieved by realizing that, at each grid point, both the weight function $w(\mathbf{r})$ and its gradient vanish in case all *constraint* atoms are beyond the cutoff radius. This follows from the fact that the corresponding cell functions and, by extension, their gradients are in this

instance identically zero (compare with Equations (9) and (11)). Therefore, the constraint is nonzero only inside a space defined by the superposition of spheres with a radius equal to the cutoff radius centered on the constraint atoms. A number of algorithms can in principle be employed to construct such a confinement cavity. Inspired by various continuum solvation models, an implementation relying on a spherical Gaussians $g_i(\mathbf{R}_i, r_i^{\text{gauss}})$ has been developed. Specifically, the cavity is constructed by first summing the Gaussians $\sum_{i \in \mathcal{W}} g_i(\mathbf{R}_i, r_i^{\text{gauss}})$, and then by discarding any grid points where the Gaussian density falls below a predetermined screening cutoff, as illustrated in Figure S7. The width of these Gaussians is controlled by a radius parameter r_i^{gauss} , and we have found that using van der Waals radii results in the most efficient confinement. Finally, it should be noted that the functions defining the constraint satisfy particular pairwise symmetry relations. Thus, once the atom pair ij , $i < j$, has been calculated, there is actually no need to compute the reverse pair ji . The required symmetry relations to adopt this scheme are derived in Appendix B.

2.3 CDFT Algorithm for Simultaneous Treatment of Two ET States

It is worth reiterating that evaluating the ET parameters in the Marcus rate equation (1) with CDFT boils down to sampling ΔE (Equation (6)) and $|H_{ab}|$ during molecular dynamics simulations. Specifically, at every MD time step, it is necessary to solve the constrained electronic structures of both the initial and final states of the reaction. These MD simulations must be performed twice, propagating the system with forces derived alternatively from the initial or final state, in order to evaluate the free energy quantities of Equations (7)-(8). Having introduced a number of improvements to the Becke density partitioning method in Section 2.2, we are now in a position to present our algorithm for efficient CDFT MD simulations. The key fact to observe here is that atomic positions in the two ET states are always identical since the vertical energy gap ΔE is sampled. This allows us once again to utilize the $\rho(\mathbf{r})$ insensitivity of the Becke weight function, and to construct a shared weight function and gradients for both ET states, thus avoiding wasting computational resources

on building the constraint twice.

Now, we have the option of either treating the ET states sequentially or in parallel. The latter choice is obviously superior in terms of wall clock time expended for the simulation, although it requires introducing an additional communication step to copy the constraint onto the processor subgroups handling the individual ET states. The resulting parallel algorithm has been schematically depicted in Figure 1. Another advantage of this scheme is that it enables doubling the processor count used for the calculation, further mitigating the cost of the Becke method. To improve scalability, dynamic load balancing has been incorporated into the algorithm, where the computational load is approximated using the Gaussian confinement cavity and the load prediction error from the previous MD step. Some code specific modifications to the SCF procedure were also necessary, because CP2K employs the orbital transformation (OT) method⁴⁸ to recast diagonalization of the Kohn-Sham eigenequation into solving a minimization problem by using a two tiered SCF approach. In brief, a third SCF layer has been added for constraint Lagrangian optimization to avoid interference with OT. Furthermore, the rebuild of the OT minimization preconditioner is prevented when near convergence, saving computational resources especially using the most effective, diagonalization based preconditioner.⁶²

Obviously, the superior performance of the introduced parallel algorithm hinges on the assumption that the electronic structures of both ET states converge at a roughly equal rate, since otherwise computer time is wasted while half of the processors remain idle and wait for the rest to finish. An extensive analysis on the convergence properties of the algorithm is presented in the Supporting Information based on CDFT MD simulations of various solvated systems, see in particular Figures S1-S6. To summarize, these tests show that the convergence generally depends on system, e.g. the nature of the donor and acceptor as well as the solvent environment, but within reasonable performance imbalance limits the convergence is smooth enough to justify parallelization over ET states when the system is treated entirely at the DFT level. Convergence for hybrid CDFT/MM simulations is not as good

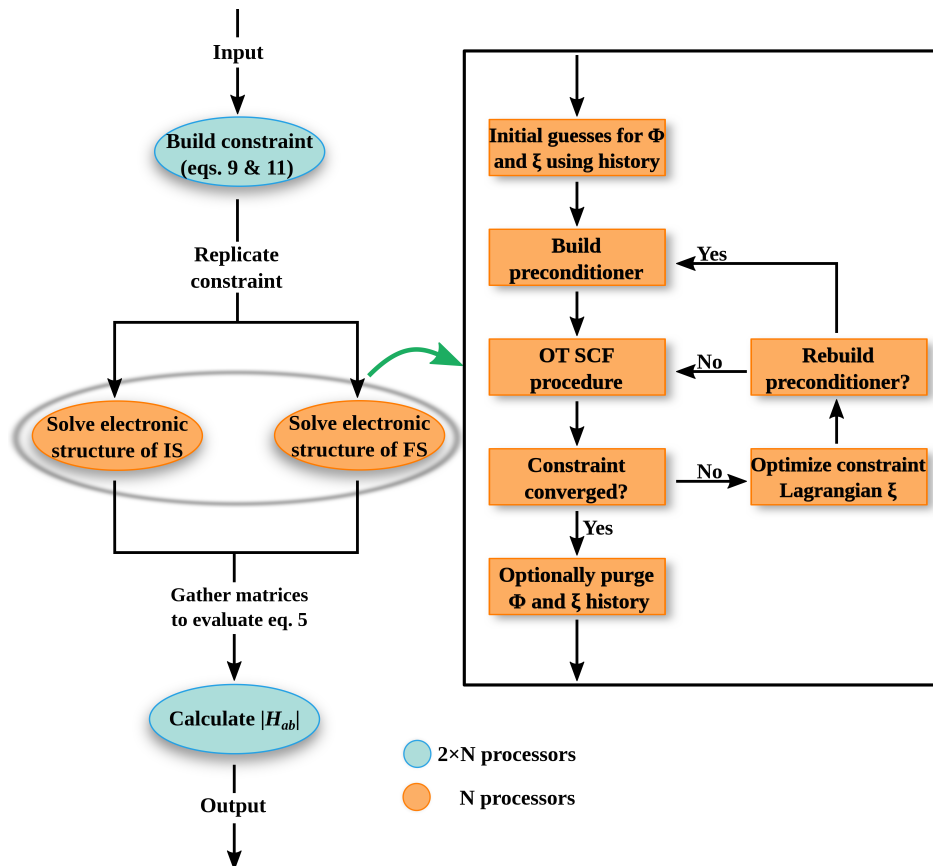


Figure 1. Parallel CDFT algorithm for the concurrent simulation of two ET states. The constraint is first built using $2N$ processors and then copied onto two processor groups of size N , which solve the constrained electronic structures of the ET initial (IS) and final (FS) states in parallel, returning the necessary matrices to calculate $|H_{ab}|$. In the constraint replication step, global MPI communication is employed to map the constraint real space grids distributed on $2N$ processors to two sets of grids on N processors. The inset shows how the CDFT constraint optimization has been incorporated into an orbital transformation⁴⁸ (OT) based electronic structure solver.

and would benefit from a serial treatment of the ET states, however; this alternative has not been considered in this work since the algorithm has mainly been designed with full DFT simulations in mind. Nonetheless, we will reevaluate our position on this matter in future applications of the presented method.

In any case, the convergence of the individual ET states is noticeably faster during MD than it would be in a series of single point calculations using the same MD snapshots, because high order extrapolation⁶³ of the state specific wavefunctions significantly accelerates convergence during MD. A multilinear extrapolation is analogously employed to improve

the initial guess accuracy of the constraint Lagrangian ξ , reducing the number of needed iterations to optimize ξ . For improved MD stability, it also helps to purge the wavefunction and ξ histories in case convergence issues are encountered. In light of these observations, it is not surprising that the performance of the CDFT algorithm in Figure 1 is superior to modeling the ET states separately while keeping the sampling frequency constant, i.e., running the CDFT MD simulation in just one ET state and subsequently calculating the other state as a series of single point computations, especially as both states are regardless required to compute $|H_{ab}|$. The latter strategy will naturally be cheaper if fewer than every MD snapshot are selected for analysis, but owing to the loss of constraint and wavefunction history, we expect that separation between subsequent configurations needs to exceed at least 20 time steps for a noticeable improvement.

We have benchmarked the performance of our CDFT method by studying intramolecular ET in the tetrathiafulvalene-diquinone radical anion (Q-TTF-Q $^{\bullet-}$) solvated in 258 water molecules, as shown in Figure 2. Specifically, we have compared the computational cost of building the constraint (weight function and its gradient) using the original Becke method with modified versions where the improvements of Section 2.2 are introduced in stages, as well as the parallel algorithm that simultaneously operates on two ET states. A considerable 97 % decrease in computational cost is achieved when all modifications are incorporated into the method, bringing the cost down to 4.7 s from 134.7 s with Gaussian confinement accounting for the majority of the observed improvement. To put these values into perspective, the average cost of an SCF iteration is around 1.3 seconds (without OT preconditioner rebuild), which underlines the reason why the original method is ill-suited for dynamic simulations. We again wish to emphasize that these modifications have no influence on the accuracy of the results. Switching over to the parallel algorithm incurs a marginal two second communication overhead that is partly negated by the introduction of load balancing which has not been implemented in the other methods. More importantly, the algorithm achieves an MD performance of 48 seconds/timestep when averaged over a 12 ps (24000 steps) long trajectory

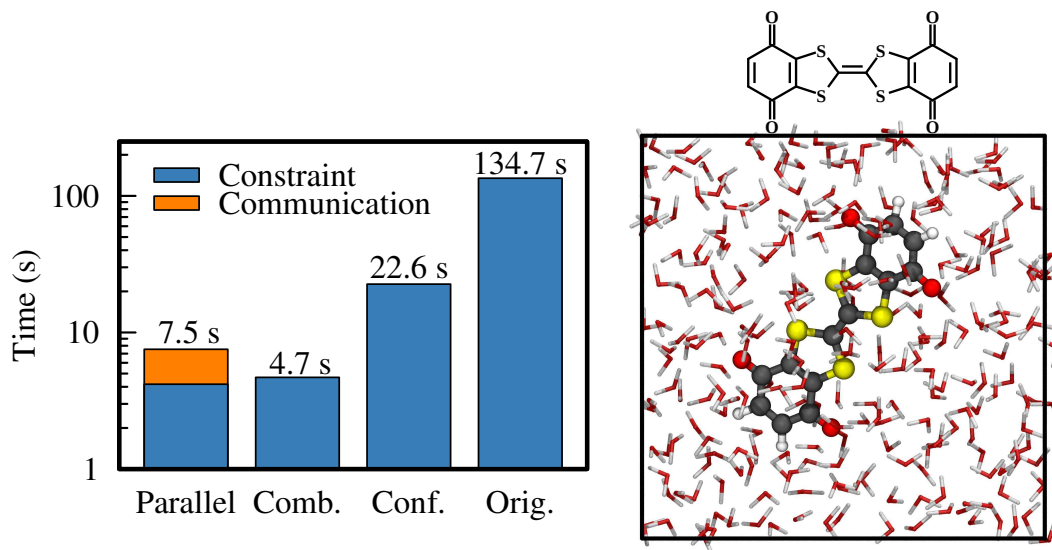


Figure 2. Benchmark calculation comparing the performance of the original Becke method (Orig.) with modified versions (Conf., Comb.) of the method as well as the parallel algorithm from Figure 1 (left). Here, ‘Conf.’ denotes the Becke method using Gaussian confinement and symmetry relations, and in ‘Comb.’ the weight function and gradient are additionally computed in one shot, see main text for additional details. Note that the constraint building kernel in the parallel algorithm is equivalent to ‘Comb.’ with the exception that dynamic load balancing is incorporated only into the former. Reported timings are for the construction of the Becke weight function and its gradient in a system composed of a tetrathiafulvalene-diquinone radical anion (Q-TTF-Q \bullet^-) solvated in 258 water molecules (right) using 384 cores of a Cray XC40. The anion is in ball-and-stick representation, with carbon depicted in gray, oxygen in red, sulfur in yellow, and hydrogen in white.

(see Section 4.3 for additional details), demonstrating that the method is indeed fully viable for carrying out two ET state condensed phase CDFT MD simulations.

3 Computational Methods

We have implemented the proposed CDFT method into a local development version of the CP2K^{50,51} code, which is available upon request from the authors until the modifications are merged into the main development version of the code. All calculations have been performed using the spin dependent formalism of the hybrid Gaussian and (augmented) planewaves method.^{49,64} Valence electrons were represented with molecularly optimized Gaussian basis sets of double ζ plus polarization quality (MOLOPT-DZVP-SR),⁶⁵ while ionic cores were

treated with norm conserving GTH-pseudopotentials,⁶⁶⁻⁶⁸ unless otherwise stated. The planewave basis was truncated with a 500 Ry energy cutoff. The Kohn-Sham equations were solved using the orbital transformation⁴⁸ method combined with a diagonalization based preconditioner,⁶² and matrix diagonalizations were accelerated with the ELPA⁶⁹ library. DFT-D3⁷⁰ van der Waals corrections with Becke-Johnson damping⁷¹ have been used throughout. The majority of the calculations were carried out with the PBE⁷² and PBE0⁷³ exchange-correlation functionals, but some tests with the BLYP^{74,75} and B3LYP⁷⁶ functionals were also performed. For condensed phase PBE0 calculations, a truncated version⁷⁷ of the functional (PBE0-TC-LRC) was employed together with the auxiliary density matrix method.⁷⁸

Vacuum phase calculations of $|H_{ab}|$ and charge transfer energies in small molecular complexes were used to validate the CDFT implementation (see Section 4 for details on the studied systems). The complexes were centered in cubic boxes with at least 10 Å vacuum surrounding the molecules in each direction, and interactions between periodic copies of the system were decoupled with the Martyna-Tuckerman⁷⁹ method. For CDFT MD simulations of Q-TTF-Q^{•-}, a fully periodic solvated system with 258 water molecules was prepared by equilibrating the solution for 1 ns in the NPT ensemble at 300 K and 1 bar using a classical forcefield, with additional details reported in the Supporting Information. The final edge length of the cubic box was 19.5510 Å. A 2+10 ps long CDFT MD trajectory was acquired in the NVT ensemble by propagating the ionic cores with the Velocity Verlet algorithm using a time step of 0.5 fs and the Bussi et al.⁸⁰ thermostat with a target temperature of 330 K. For comparison, the system was also modeled with a combined CDFT/MM MD approach using a Gaussian expansion of the electrostatic potential^{81,82} to describe the QM/MM coupling, see Supporting Information for a more comprehensive account.

In every system, the constraint has been defined as the charge difference between acceptor and donor fragments, and the appropriate target value N_c for the constraint is calculated from the number of valence electrons on the fragments, except for simulations using a non-

interacting reference state (see Equation (3)). The validation simulations were conducted with different functional forms of the Becke weight function to quantify the effects of atomic size adjustments and using isolated fragments in defining the constraint. As most of the studied systems are composed of covalent molecules, the additive atomic radii of Pyykkö and Atsumi^{83,84} have been adopted to adjust the Becke cell boundaries, using single bond radii for all elements except carbon for which the double bond value was used. For the system with a Cl⁻ anion, the impact of using Shannon’s⁸⁵ effective ionic radius for Cl was also investigated. A screening threshold of 10^{-6} was employed to construct the Gaussian confinement cavity. The constraint convergence criterion was set to $10^{-4}e$. To accelerate the CDFT MD simulations, the convergence criterion was loosened to $10^{-2}e$ as we did not observe any degradation of results in short test simulations, and the average drift of the MD conserved quantity remained reasonable ($-0.7 \mu\text{Ha ps}^{-1} \text{atom}^{-1}$ over a 10 ps trajectory). Element specific cutoff radii were set to 2.65 Å for elements heavier than H, while 2.28 Å was used for H.

4 Results and Discussion

The CDFT implementation has been validated using a twofold approach, testing in both instances how sensitive the results are to the choice of weight function, DFT functional, and basis set. We have first evaluated the method’s accuracy for calculating $|H_{ab}|$ values by comparison to high level ab initio reference values for hole transfer in helium, zinc, and small organic molecule dimers, and for electron transfer between benzene and a neutral chlorine atom. Subsequently, charge transfer energies are computed for a set of twelve molecular complexes which are benchmarked against reference CDFT values obtained with a different weight function. We then present our results on the condensed phase CDFT MD simulations of Q-TTF-Q^{•-} and conclude with a brief analysis regarding the influence of computational parameters on the quality of CDFT results.

4.1 Validation of Electronic Couplings

As the first test of our method, we have calculated $|H_{ab}|$ for the electron transfer reaction between benzene and a neutral chlorine atom, $\text{C}_6\text{H}_6 + \text{Cl} \rightleftharpoons \text{C}_6\text{H}_6^+ + \text{Cl}^-$, using various weight functions and two exchange-correlation functionals. This system presents a stringent test for CDFT due to nonnegligible overlap between the donor and acceptor, which combined with the availability of high level ab initio GMH data¹⁵ has made it a prime benchmark case for CDFT implementations.^{22,23} Following Cave and Newton,¹⁵ the Cl atom is placed 3 Å above the benzene molecular plane at distances, d , 0.604 Å and 1.208 Å away from the six-fold symmetry axis of benzene in the direction of a C-C bond bisector. The calculated $|H_{ab}|$ values are summarized in Table 1. Focusing first on the PBE results, an excellent agreement is found between reference GMH¹⁵ values and our CDFT calculations with the Becke weight where cell boundaries are shifted using covalent radii for C and H and the ionic radius of Cl (BW+A* weight). The values are also consistent with prior CDFT results reported by Wu and Van Voorhis²² using an all-electron local basis set approach and the Becke weight as well as by Oberhofer and Blumberger²³ employing planewaves and the Hirshfeld weight. The agreement with GMH values worsens when atomic radii are employed for all elements (BW+A weight), whereas neglecting the atomic size correction (BW weight) causes $|H_{ab}|$ to erroneously vanish for $d = 1.208$ Å due to the two ET states becoming numerically orthogonal. Moreover, the BW weight function is unable to reproduce chemically reasonable partial atomic charges for benzene-Cl in the unconstrained DFT ground state unlike the other weight functions, see Table S1.

Above, the ET states have been constructed by constraining the charge difference between benzene and Cl to satisfy the expected formal difference obtained by counting electrons on both fragments. Alternatively, isolated neutral and charged molecular fragments could be employed to define the ET states in such a way that the number of electrons on both fragments matches the calculated value in the superimposition of noninteracting reference densities, see Equation (3). Repeating the $|H_{ab}|$ calculations with fragment based Becke

Table 1. CDFT Electronic Couplings $|H_{ab}|$ for Benzene-Cl Calculated with Different Weight Functions Compared to CDFT and GMH Results from the Literature. The Tested Weight Functions Include: Becke Weight (BW), Becke Weight Adjusted with Covalent Atomic Radii (BW+A), Becke Weight Adjusted with Covalent Atomic (for C, H) and Ionic (for Cl) Radii (BW+A*), as well as the Corresponding Fragment Based Becke Weights (FBB) with Values Given in Parentheses. All Values Are in MilliHartree (mHa).

Method	Weight	$d = 0.604 \text{ \AA}$	$d = 1.208 \text{ \AA}$
CDFT PBE ^a	BW	61.2 (36.0)	0.0 (38.3)
	BW+A	28.6 (29.4)	34.6 (39.2)
	BW+A*	48.9 (47.7)	47.1 (56.8)
CDFT PBE0 ^a	BW	68.0 (28.8)	79.3 (28.9)
	BW+A	14.2 (23.8)	21.3 (31.2)
	BW+A*	52.8 (34.4)	75.2 (42.7)
GMH ^b	–	51.0	51.9
CDFT BLYP ^c	Hirshfeld	55.9	52.3
CDFT B3LYP ^d	BW	48.8	56.1

^a This work.

^b Reference 15.

^c Reference 22.

^d Reference 23.

weights preserves the quality of the results with atomic size adjustments (FBB+A/FBB+A* weights), and notably corrects the zero $|H_{ab}|$ value without size adjustments (FBB weight). Switching over to the PBE0 functional, the BW+A* weight again yields the best agreement with reference values, although $|H_{ab}|$ at $d = 1.208 \text{ \AA}$ is now overestimated, while the ordering of BW and BW+A is reversed with the former over- and the latter underestimating the electronic coupling. Using fragment densities with PBE0 lowers the FBB and FBB+A* values too much when compared to GMH values, only improving the accuracy of FBB+A values.

Based on the above analysis, it is evident that the $|H_{ab}|$ values in Table 1 vary quite considerably depending on the choice of the weight function, which stems from the difficulty of reliably partitioning the total electron density of benzene-Cl into fragment contributions due to significant overlap between fragments. This effect is by no means unique to the present CDFT implementation, c.f. Refs. 22 and 23, and highlights the importance of benchmarking

when modeling strongly interacting charge transfer systems. In fact, wavefunction based methods are prone to similar difficulties as well, exhibiting a sensitivity to the choice of basis set, electronic structure method, and the formalism employed to compute $|H_{ab}|$.⁸⁶ We shall discuss this matter further in Sections 4.2 and 4.4.

As stated earlier, we have implemented our CDFT method within the GPW⁴⁹ (GAPW⁶⁴) framework of the CP2K^{50,51} code which employs a dual basis of Gaussian functions and (augmented) planewaves. The quality of the Gaussian basis set is likely to affect the quality of calculated CDFT electronic couplings, especially when the donor-acceptor distance is increased, given the finite spatial extent of Gaussians. We have investigated the basis set sensitivity of $|H_{ab}|$ by studying hole transfer in He_2^+ and Zn_2^+ as a function of the internuclear separation with basis sets of different quality and hence vastly different computational cost: molecularly optimized double ζ plus polarisation basis sets (MOLOPT-DZVP-SR),⁶⁵ traditional split valence quadruple ζ basis set with uncontracted polarization functions (GTH-QZV3P),⁵⁰ and Ahlrichs’ def2-QZVP⁸⁷ all-electron basis set. The results have been collected into Tables S2-S3 where they have been compared to high level ab initio GMH data.^{15,88,89}

At small internuclear separations, virtually no difference between basis sets is observed, and the accuracy of $|H_{ab}|$ values is primarily determined by the exchange-correlation functional and we find a very satisfactory agreement with reference values. Quite expectedly, the $|H_{ab}|$ values start deviating when the separation is increased, with each basis set nonetheless reproducing the characteristic exponential decay of electron tunneling, $|H_{ab}| \propto \exp(-\beta r/2)$ where β is the so-called decay constant. The MOLOPT-DZVP-SR basis underestimates the coupling at largest distances leading to decay constants that are too large. Overall, the all-electron basis set most faithfully reproduces the reference GMH decay constants, at an accuracy comparable to other CDFT implementations.^{22,23} We wish to note in passing that the cutoff of the auxiliary planewave basis has a significantly smaller impact on the quality of $|H_{ab}|$; by varying the cutoff in the range 380-800 Ry, the maximum observed change in $|H_{ab}|$ relative to results with 500 Ry is 40 μHa in tested configurations.

It is not uncommon, however, for CDFT to systematically over- or underestimate $|H_{ab}|$, particularly when using GGA functionals. In comprehensive studies of charge transfer in anionic and cationic organic dimers, Blumberger and coworkers^{89,90} demonstrated that the accuracy of CDFT couplings can be improved by simply scaling the values with a functional dependent constant, obtained by fitting a linear dependence between CDFT and reference $|H_{ab}|$ values. In order to further validate our method, we have evaluated $|H_{ab}|$ values for the HAB11⁸⁹ database of stacked cationic homodimers using different weight functions and functionals. The results obtained with the MOLOPT-DZVP-SR basis set are compared to reference ab initio data^{89,91} in Table 2.

Table 2. Signed Errors of CDFT Electronic Couplings $|H_{ab}|$ (in mHa) and Decay Constants β (in $1/\text{\AA}$) for the HAB11⁸⁹ Set of Homodimer Cations Relative to High Level Ab Initio Calculations. Statistical Evaluation of Both Quantities over the Entire Dataset Is Presented for Each Weight Function-Functional Combination. Statistical Parameters after Linear Scaling of $|H_{ab}|$ Are Given in Parentheses.

Dimer	Distance	PBE			PBE0	Ref.
		BW	BW+A	FBB+A	BW+A	
Acetylene ^a	3.5	4.0	3.8	6.6	1.6	16.9
	4.0	1.5	1.5	2.7	0.4	8.5
	4.5	0.6	0.6	0.7	0.1	4.2
	5.0	0.2	0.2	0.1	0.0	2.1
	β	0.17	0.15	0.37	0.10	2.80
Benzene ^b	3.5	4.5	4.5	7.6	2.4	16.3
	4.0	1.5	1.5	3.9	0.6	8.1
	4.5	0.5	0.5	1.9	0.0	4.0
	5.0	0.2	0.2	0.7	-0.1	1.9
	β	0.19	0.22	0.11	0.26	2.84
Cyclobutadiene ^a	3.5	8.9	9.2	8.2	-0.6	17.0
	4.0	4.3	4.3	4.6	-1.6	8.8
	4.5	2.0	2.0	1.7	-1.1	4.5
	5.0	0.8	0.8	0.6	-0.7	2.3
	β	0.15	0.16	0.22	0.42	2.68
Cyclopentadiene ^a	3.5	6.9	6.7	10.3	3.1	17.1
	4.0	2.6	2.4	5.6	0.8	8.6
	4.5	0.9	0.8	2.8	0.1	4.2
	5.0	0.4	0.4	1.4	0.0	2.0
	β	0.22	0.20	-0.08	0.21	2.89
Cyclopropene ^a	3.5	8.7	8.6	13.4	4.4	19.7
	4.0	3.0	2.9	6.9	1.1	9.3

Table 2. Continued.

Dimer	Distance	PBE			PBE0	Ref.	
		BW	BW+A	FBB+A	BW+A		
Ethylene ^a	4.5	1.0	1.0	3.3	0.2	4.4	
	5.0	0.5	0.5	1.4	0.1	2.0	
	β	0.21	0.21	-0.01	0.23	3.06	
	3.5	2.9	3.0	6.7	1.0	19.1	
	4.0	1.2	1.2	3.3	0.0	10.0	
	4.5	0.5	0.5	1.3	-0.2	5.1	
	5.0	0.2	0.2	0.4	-0.1	2.5	
Furane ^a	β	0.09	0.10	0.21	0.14	2.70	
	3.5	3.8	3.7	6.9	1.4	16.2	
	4.0	1.3	1.2	3.6	0.2	7.9	
	4.5	0.5	0.5	1.7	0.0	3.7	
	5.0	0.3	0.3	0.8	0.0	1.7	
	β	0.08	0.08	-0.06	0.11	3.01	
	3.5	4.6	4.6	8.1	2.1	15.3	
Imidazole ^b	4.0	1.5	1.5	4.1	0.3	7.6	
	4.5	0.5	0.5	1.8	-0.1	3.8	
	5.0	0.1	0.1	0.6	-0.2	1.9	
	β	0.28	0.27	0.19	0.33	2.81	
	3.5	4.4	4.4	7.3	2.3	13.5	
	4.0	1.5	1.4	3.8	0.6	6.5	
	4.5	0.4	0.4	1.7	0.0	3.1	
Phenol ^b	5.0	0.1	0.1	0.7	-0.1	1.5	
	β	0.30	0.30	0.09	0.29	2.94	
	3.5	4.3	4.3	7.6	1.7	16.8	
	4.0	1.6	1.5	4.1	0.3	8.4	
	4.5	0.5	0.5	2.0	-0.1	4.1	
	5.0	0.2	0.2	0.9	-0.1	1.9	
	β	0.15	0.15	0.00	0.18	2.89	
Pyrrole ^a	3.5	6.2	6.3	9.5	3.1	16.2	
	4.0	2.2	2.1	4.9	0.7	8.1	
	4.5	0.7	0.7	2.1	0.0	4.0	
	5.0	0.2	0.2	0.7	-0.1	2.0	
	β	0.28	0.28	0.20	0.32	2.81	
	Thiophene ^b	MUE (mHa)	2.1	2.1	3.8	0.8	
			(0.6)	(0.6)	(0.5)	(0.5)	
MRSE (%)		22.1	21.7	47.1	2.1		
		(-6.0)	(-6.1)	(-2.0)	(-6.9)		
MRUE (%)		22.1	21.7	47.1	7.8		
		(9.5)	(9.7)	(7.9)	(8.9)		

Table 2. Continued.

Dimer	Distance	PBE			PBE0	Ref.
		BW	BW+A	FBB+A	BW+A	
β	MAX (mHa)	8.9 (2.9)	9.2 (3.2)	13.4 (2.4)	4.4 (2.2)	
	MUE (1/Å)	0.19	0.19	0.14	0.23	
	MRSE (%)	6.7	6.7	4.1	8.3	
	MRUE (%)	6.7	6.7	5.0	8.3	
	MAX (1/Å)	0.30	0.30	0.37	0.42	

^a MRCI+Q reference⁸⁹

^b MBPT(2) reference⁹¹

According to Table 2, PBE in conjunction with the BW or BW+A weight function overestimates the reference electronic couplings, giving mean relative signed and unsigned errors (MRSE/MRUE) of 22 % when averaged over the entire HAB11 dataset. Because here the charge acceptor and donor are identical, perfectly stacked molecules, using atomic size adjustments in the construction of the Becke weight function has a negligible effect on calculated values even at short distances. By contrast, the couplings become further overestimated with the fragment based Becke weight resulting in a MRSE and MRUE of 47.1 %. Switching to the PBE0 functional (BW+A weight) systematically improves the couplings, decreasing MRSE to 2.1 % and MRUE to 7.8 %. For this particular dataset, increasing the fraction of exact exchange would likely lead to an even better agreement with reference values,⁸⁹ but this is not required to validate our method and has thus not been explored. Interestingly, the relative ordering of these methods is reversed when the accuracy of the exponential decay constants is examined, with PBE/FBB+A yielding the smallest MRUE, 5.0 %, and PBE0/BW+A the largest, 8.3 %.

A scatter plot of CDFT and reference $|H_{ab}|$ values reveals that their correlation is indeed linear ($R^2 \approx 0.99$), as illustrated in Figure S8 for the PBE/BW+A data. A notable improvement in the statistical parameters of PBE/BW+A is observed after uniformly scaling the couplings with the inverse slope of the linear dependence (see Figure S8 for numerical

values), decreasing MRSE to -6.0 % and MRUE to 9.5 %. Equal improvements are obtained with other weight functions and the PBE functional. On the other hand, no statistical improvement is gained by scaling the PBE0 values, which was to be expected as the scaling factor (0.9114) is close to unity.

4.2 Validation of Charge Transfer Energies

CDFT has recently been applied to probe charge transfer (CT) energies in noncovalent complexes.⁹²⁻⁹⁴ Extracting the CT energy, $-\Delta E_{CT}$, from the total interaction energy is often challenging theoretically (see e.g. Ref. 95 for a recent review), but in the CDFT framework, it is conveniently defined as the energy difference of the complex with a fully relaxed electron density, E_{DFT} , and with a relaxed density where CDFT is employed to prevent charge transfer between the complex fragments, E_{CDFT} ,⁹²

$$-\Delta E_{CT} = E_{CDFT} - E_{DFT} \tag{12}$$

The set of 11 CT complexes originally proposed by Hobza and coworkers⁹⁶ and later adapted to CDFT CT calculations by Řezáč and de la Lande⁹² is particularly interesting for method validation purposes because it includes complexes with strongly overlapping fragments, spanning a wide range of CT energies. CDFT is known to struggle for complexes where the fragment electron densities overlap, since in this limit it is no longer possible to uniquely partition the total density into fragment contributions,⁵⁶ which we have already discussed in relation to benzene-Cl system in Section 4.1. Indeed, the authors⁹² demonstrated that all commonly used weight functions, including BW, Hirshfeld, and orbital dependent weights, predicted inconsistent CT energies over the set of complexes. A reliable estimate of $-\Delta E_{CT}$ was made possible only by using a weight that reflected the actual electronic structure of the isolated molecular fragments, $\tilde{\rho}_i$. This weight, dubbed ‘fragment based Hirshfeld’ (FBH), is defined through

$$w_{\text{FBH}}(\mathbf{r}) = \frac{\tilde{\rho}_A(\mathbf{r})}{\tilde{\rho}_A(\mathbf{r}) + \tilde{\rho}_B(\mathbf{r})} \quad (13)$$

and should be contrasted to the original Hirshfeld⁵⁹ weight where isolated atomic densities are used instead of $\tilde{\rho}_i$. In a subsequent study,⁹³ fragment based Voronoi and Becke weights were shown to perform comparably to the FBH weight, although the authors eventually advocated the usage of FBH due to overall smaller CT energies. We have validated our CDFT implementation against this data set with the addition of a water dimer system, taken from the S66⁹⁷ data set. The computed PBE/MOLOPT-DZVP-SR charge transfer energies are collected into Table 3 where they are compared to PBE0/def2-QZVP results⁹³ obtained with the FBH weight.

Table 3. Comparison between PBE/MOLOPT-DZVP-SR Charge Transfer Energies (in mHa), $-\Delta E_{\text{CT}}$, Computed Using Different Weight Functions and Reference Values Obtained with the Fragment Based Hirshfeld Weight Function at the PBE0/def2-QZVP⁹³ Level of Theory. The Magnitude of Charge Transferred between Fragments, $|\Delta q|$, in the Unconstrained Ground State Is Also Shown. For the FBB+A Weight, $|\Delta q|$ Is Relative to the Superposition of the Isolated Fragments. The Difference between Constraint Target Values with the BW+A and FBB+A Weights, $\Delta N_c = N_c - \tilde{N}_c$, Are Reported.

System	$-\Delta E_{\text{CT}}$				$ \Delta q $			$ \Delta N_c $
	Ref.	BW	BW+A	FBB+A	BW	BW+A	FBB+A	
H ₂ O – H ₂ O	1.7	45.9	1.1	2.1	0.29	0.03	0.04	0.01
C ₂ H ₂ – ClF	2.0	0.0	41.1	3.9	0.01	0.48	0.15	0.33
C ₂ H ₄ – F ₂	0.6	5.1	12.0	2.1	0.13	0.18	0.10	0.09
H ₂ O – ClF	2.9	2.4	73.8	4.0	0.10	0.47	0.12	0.36
HCN – ClF	1.3	0.3	21.9	1.8	0.03	0.31	0.08	0.23
NH ₃ – BH ₃	18.5	81.1	175.8	25.5	0.73	1.14	0.40	0.74
NH ₃ – Cl ₂	4.2	0.1	67.4	5.6	0.02	0.53	0.18	0.35
NH ₃ – ClF	11.6	0.1	104.5	13.2	0.03	0.76	0.29	0.47
NH ₃ – F ₂	1.1	10.7	20.6	3.5	0.18	0.23	0.13	0.10
NH ₃ – SO ₂	3.0	0.2	55.9	2.8	0.03	0.42	0.11	0.31
NMe ₃ – BH ₃	20.0	63.0	153.3	27.0	0.74	1.20	0.47	0.73
NMe ₃ – SO ₂	20.8	0.0	132.6	18.9	0.00	1.07	0.43	0.64
MUE (mHa)		17.2	64.4	2.3				
MSE (mHa)		10.1	64.4	1.9				
MAX (mHa)		62.6	157.2	7.0				

It is immediately obvious that both the BW and BW+A weights are unable to precisely describe CT energies in the investigated systems. On average, BW+A overestimates the CT energies by 64.4 mHa (MSE/MUE), while BW performs marginally better with a MUE of 17.2 mHa. The statistical accuracy of these methods show no improvement upon changing to a larger GTH-aug-QZV3P basis set (Table S4) or by switching over to the PBE0 functional (Table S5). By contrast, the fragment based Becke weight is in satisfactory agreement with the PBE0/FBH reference values already with the MOLOPT-DZVP-SR basis, as verified by the 2.3 mHa MUE and -1.9 mHa MSE, and further improves with the larger basis and the PBE0 functional (Tables S4-S5).

To understand why the BW and BW+A weights perform poorly, it is instructive to examine the magnitude of charge transferred, $|\Delta q|$, between the molecular fragments in the unconstrained DFT ground state. Table 3 shows BW+A predicts that a notable amount of charge is transferred in the majority of the systems, exceeding one electron in the datively bonded BH_3 complexes and $\text{NMe}_3 - \text{SO}_2$. Correlating these values to the CT energies reveals a dependence that grows quite linearly with increasing $|\Delta q|$, see Figure S9. The degree that BW+A overestimates $|\Delta q|$ values is simple to gauge by comparison to the respective FBB+A values, which is analogously described by the difference in constraint target values $\Delta N_c = N_c - \tilde{N}_c$ also shown in Table 3. This metric demonstrates severe, on average 60 %, overestimation of $|\Delta q|$ values, ultimately causing the erroneous CT energies, and thus highlights the importance of accounting for isolated fragment densities in this particular application where the overlap between fragments is considerable. Here, BW happens to outperform BW+A by virtue of smaller $|\Delta q|$ prediction errors (see Tables S4-S5), but once again the BW atomic partial charges are chemically unrealistic (see Table S6).

4.3 Condensed Phase CDFT MD Simulation of Q-TTF-Q \bullet^-

Q-TTF-Q \bullet^- is a prototypical example of a mixed valence compound (see also Figure 1) that has been difficult to classify either as class II or III in the Robin-Day⁹⁸ classification scheme,

where molecules are categorized according to the strength of the electronic coupling $2|H_{ab}|$. Experimentally, Q-TTF-Q \bullet^- exhibits class II behavior in a 10:1 mixture of ethyl acetate and tert-butanol,⁹⁹ i.e., the excess electron is partly localized onto one of the quinone rings but can transfer back and forth between the two rings, as the electronic coupling is nonzero but smaller than the solvent reorganization energy ($2|H_{ab}| < \lambda$). The accurate description of this anion has posed a considerable challenge for theoretical studies.^{22,23,40,43,100–103} In vacuum, common GGA and hybrid functionals predict that the excess electron is fully delocalized, which is characteristic of class III compounds ($2|H_{ab}| > \lambda$). In light of the contradicting experimental observation, this result has often been (mis)interpreted as a manifestation self-interaction error, and class II behavior has been enforced by e.g. using long-range corrected hybrid functionals^{100,101} or through CDFT approaches.^{22,23,40,43} More recently, Renz and Kaupp¹⁰² questioned this interpretation and demonstrated delocalized character with the BLYP35 functional (35% exact exchange), which has been validated against a variety of other mixed valence compounds.^{36,104–106} The authors were also able to show that correct class III behavior is recovered only in polar solvents using continuum solvation and D-COSMO-RS models.

With the vast amount of CDFT and other theoretical data available, we have selected Q-TTF-Q \bullet^- as a model system to test the implementation of our parallel CDFT algorithm for condensed phase MD simulations. Previous vacuum calculations have also been reproduced for comparison. As expected, unconstrained vacuum optimization of Q-TTF-Q \bullet^- at the PBE level results in a perfectly symmetrical structure with the excess electron delocalized over the whole molecule. By enforcing charge localization, a small energy gap of $\Delta E = 20.8 \mu\text{Ha}$ ($\Delta E = 20.5 \mu\text{Ha}$ for PBE0) is observed between the two diabatic states, consistent with the $31 \mu\text{Ha}$ B3LYP energy gap reported by Oberhofer and Blumberger.²³ A similar agreement is found between calculated CDFT couplings $|H_{ab}|$ at this configuration: we obtained values of 16.9 mHa for PBE and 3.6 mHa for PBE0, respectively, while previously reported values include 4.9 mHa (B3LYP),²² 11.2 mHa (BLYP), 3.8 mHa (B3LYP),²³ 4.4 mHa (BLYP35),¹⁰²

as well as the experimental estimate of 0.7 mHa.⁹⁹ The experimental value was calculated from the Marcus rate equation (1) using the measured ET rate constant ($1.3 \times 10^8 \text{ s}^{-1}$) and activation free energy ($6.4 \text{ kcal mol}^{-1}$) in a 10:1 mixture of ethyl acetate and tert-butanol;⁹⁹ precipitation of Q-TTF-Q \bullet^- has made it impossible to quantify the reaction in other solvents.

To investigate how the inclusion of solvent affects intramolecular ET in Q-TTF-Q \bullet^- , a CDFT MD simulation of the molecule was carried out in a system with 258 explicit water molecules using the PBE functional, sampling ΔE every step (0.5 fs) and $|H_{ab}|$ every 10 fs. Data was collected for a total of 10 ps, following initial classical and CDFT equilibrations. Comparison calculations with the PBE0 functional were performed by extracting snapshots from the PBE trajectory every 0.125 ps and performing single point calculations on these configurations. In another series of calculations, all water molecules were stripped from these snapshots and the ET parameters were reevaluated in vacuum with both functionals. Finally, a mixed CDFT/MM MD simulation of the system was also conducted, see Supporting Information for further details.

The time evolution of ΔE and $|H_{ab}|$ are depicted in Figure 3 for the CDFT MD simulation with explicit water molecules, while the corresponding results are shown in Figures S10-S11 for the vacuum configurations and CDFT/MM simulations. Unsurprisingly, a considerable increase in the vertical energy gap is observed when compared to the vacuum calculation in the symmetric minimum energy configuration, because the excess electron localized on one of the quinone rings becomes stabilized by surrounding water molecules, be it explicit quantum mechanical or mixed QM/MM representation. The same effect is apparent in the data where Q-TTF-Q \bullet^- configurations are extracted from the MD trajectory and placed in vacuum (Figure S10). For ΔE , there is no perceivable difference between functionals and overall the PBE0 values follow the trend of the PBE data. On the contrary, the hybrid functional predicts noticeably smaller $|H_{ab}|$ values than PBE in all considered approaches. Here, the sharp drops in $|H_{ab}|$ can be attributed to the two charge localized states becoming momentarily orthogonal, see Figure S12.

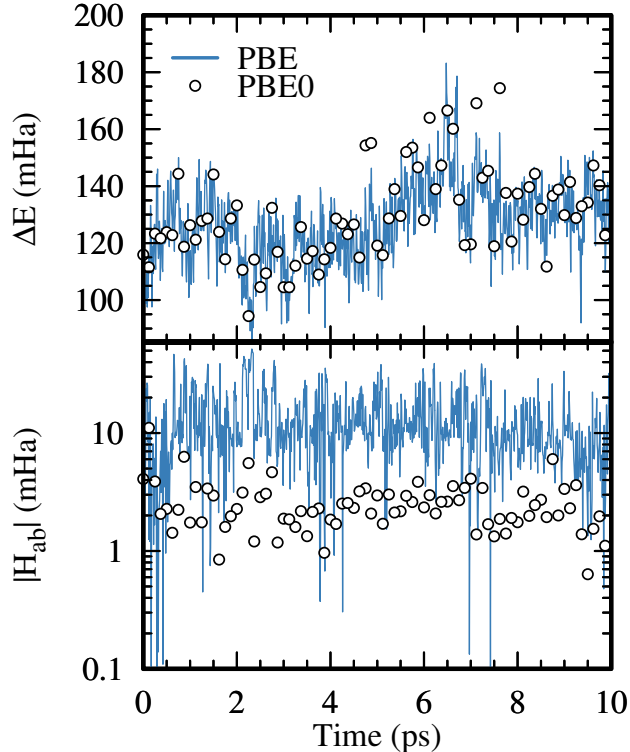


Figure 3. Time evolution of ΔE (top) and $|H_{ab}|$ (bottom) during a CDFT MD simulation of Q-TTF-Q \bullet^- in water. The PBE functional was used for generating the MD trajectory, while PBE0 values are single-point calculations on equidistantly spaced snapshots.

As the Marcus rate equation (1) suggests, the key parameters describing the intramolecular ET process of Q-TTF-Q \bullet^- are the quadratic mean $\langle |H_{ab}|^2 \rangle_T^{1/2}$ and the solvent reorganization free energy λ . Because Q-TTF-Q \bullet^- is a symmetric molecule, it is sufficient to compute a single MD trajectory to characterize these parameters. In particular, substitution of $\langle \Delta E_A \rangle_T = -\langle \Delta E_B \rangle_T = \langle \Delta E \rangle_T$ into Equations (7)-(8) yields $\Delta A = 0$ and λ is simply given by the average vertical energy gap, $\langle \Delta E \rangle_T$. These parameters have been assessed for all computational approaches and are collected into Table 4.

For both functionals, the thermal averages of $|H_{ab}|$ are slightly lower than the values obtained at the unconstrained PBE minimum energy configuration, consistent with observations of Renz and Kaupp¹⁰² using implicit solvent models. Although the PBE0 computed mean, 3.0 mHa, is larger than the 0.7 mHa estimate derived from experiments, the agreement can nonetheless be considered satisfactory given the difference in solvents (see also additional

Table 4. Electron Transfer Parameters for Intramolecular ET in Q-TTF-Q^{•-} Solvated in Water Obtained with CDFT and CDFT/MM Approaches Using the PBE and PBE0 Functionals. Parameters from Vacuum Simulations Are Given in Parentheses. Error Estimate Is the Difference between Parameter Values in Two Halves of the Trajectories. Values in mHa.

Property	CDFT		CDFT/MM	
	PBE	PBE0	PBE	PBE0
$\langle H_{ab} ^2 \rangle^{1/2}$	15.4 ± 3.3 (9.9 ± 1.0)	3.0 ± 0.6 (3.2 ± 0.7)	11.1 ± 4.5	3.2 ± 0.1
λ	126.9 ± 14.3 (22.3 ± 2.8)	129.8 ± 16.9 (26.7 ± 3.5)	134.2 ± 2.9	143.0 ± 3.8

discussion below). We find PBE overestimates the PBE0 electronic coupling by a factor of 5, which is partly explained by the greater overlap between diabatic states with PBE (Figure S12). Stripping the solvent molecules from the system or using a CDFT/MM approach both decrease the electronic coupling with PBE, whereas the PBE0 value remains unaltered. The interaction of Q-TTF-Q^{•-} and water has previously been investigated by Blumberger and Oberhofer,²³ who performed an unconstrained MD simulation of the system and subsequently sampled $\langle \Delta E \rangle_T$ and $|H_{ab}|$ from snapshots of the trajectory. The latter quantity was evaluated by removing all water molecules from the snapshots, yielding a thermal average of 6.7 mHa with the B3LYP functional, or roughly double the present PBE0 value.

Focusing our attention next on the solvent reorganization energy, λ , it is evident that all approaches predict a consistent value of approximately 130 mHa in water. This value decreases considerably to 25 mHa once the water molecules are removed, which again illustrates the ability of water to stabilize the charge localized state. By contrast, Blumberger and Oberhofer²³ obtained a value of 8.9 mHa with B3LYP in water, which is understandably smaller than our estimate because, contrary to simulations herein, the authors did not enforce charge localization during MD. Unfortunately, it is possible to compare λ to experiments only on a qualitative level, since the aforementioned solubility issues prevent an estimation of λ in water. Regardless, measured NIR spectra for Q-TTF-Q^{•-} in a 10:1 mixture of ethyl acetate and tert-butanol reveal a broad charge transfer band associated with

the intramolecular ET process at 1300 nm,⁹⁹ which after a change of units results in $\lambda = 35$ mHa. An alternative and slightly larger estimate of 41 mHa is obtained directly from the fitted activation free energy, as determined by temperature-dependent ESR spectroscopy.⁹⁹ Both of these values are roughly a third smaller than our water estimate; however, the hydration properties of water and ethyl acetate/tert-butanol are radically different, resulting in a solvent-QTTF-Q^{•-} interaction that is notably stronger in water owing to the high polarity and small size of water. In this respect, the difference in λ to experimental values does not seem as significant, but the present data permits no further speculation on the matter.

4.4 Influence of Computational Parameters on the Accuracy of CDFT Results

The numerical examples considered in Sections 4.1-4.3 have demonstrated that the implemented CDFT algorithm can efficiently and accurately be applied to investigate a variety of charge transfer related phenomena. However, the quality of the results may exhibit sensitivity to choice of weight function (atomic size adjustments, constraint reference state) and computational parameters (functional, basis set) depending on the studied system, which has been reported in earlier CDFT literature³⁰ but is a matter we believe nonetheless warrants further discussion.

In this context, it is important to distinguish between two classes of CT systems where CDFT is applied to model either both (Sections 4.1 and 4.3) or only of one (Section 4.2) of the states involved in the CT process. The former case is generally less prone to methodical errors, and a natural parameter choice for overall best quantitative precision is to select a hybrid functional and use it together with the atomic size adjusted Becke weight. The choice of basis set is not as crucial, becoming vital only in the limit of widely separated, weakly interacting fragments. Typically, GGA functionals are also perfectly adequate for examining such systems, at least on a semiquantitative level, and their accuracy may be improved through scaling strategies.

On the other hand, systems with strongly overlapping fragments should always be treated with extra scrutiny and require a careful benchmarking of the computational parameters. The same conclusion applies to CT phenomena where the absolute energy of a CDFT state is compared to a reference state modeled with a different approach. In these instances, using isolated reference states to define the constraint instead of a formal charge based prescription is beneficial in case a priori determination of fragment charges is unreliable due to significant overlap between fragments, see Section 4.2 and Refs. 57,58,92,93 for additional examples. We recommend using atomic size adjustments even for the fragment based Becke weight function because obtaining chemically realistic partial atomic charges is impossible without it.

5 Conclusion

In this work, we have presented a well-scaling constrained DFT implementation within the computational framework of the hybrid Gaussian and planewaves method and the orbital transformation electronic structure solver. The accuracy of our method was validated against ab initio wavefunction and other theoretical results for predicting electronic couplings and charge transfer energies of gas phase complexes. Unlike the majority of prior CDFT implementations, the current method can simultaneously operate on both diabatic states involved in an electron transfer reaction and to propagate these states during a constrained molecular dynamics simulation, making the method ideally suited to investigate dynamical charge transfer phenomena such as solvation effects. We have specifically opted to solve the two states in parallel to maximize throughput, although a serial mode modification of the algorithm is possible in future applications of the method in case parallel converge issues arise, which is a strategy that has enjoyed success in hybrid CDFT/MM simulations.^{40,41} By adopting these design criteria, the implementation allows the characterization of all ET parameters directly from CDFT MD simulations, and at the same time remains sufficiently efficient in

terms of computational cost to enable the usage of an accurate, electronic structure based description of the solvent. To demonstrate this capability, we studied the intramolecular ET reaction of Q-TTF-Q^{•-} in ca. 260 explicit water molecules, which yielded ET parameters that were in agreement with experimental values in another solvent.

To summarize, the reported implementation thus successfully extends the applicability of CDFT to larger systems. This is appealing in a number of applications, chief among them biologically motivated ET processes where interesting system sizes often contain hundreds of atoms, and the prospect of dynamically modeling these reactions entirely at the electronic structure level has in previous implementations been effectively prevented by the insurmountable computational cost of treating such large systems.

Acknowledgement

We thank Dr. Florian Schiffmann for implementing the initial version of CDFT in CP2K (unaltered Becke weight/SCF structure), Drs. Andreas Marek and Lorenz Hüdepohl for their help in setting up the ELPA library, and Dr. Jan Řezáč for providing geometries for the CT complexes in Section 4.2 from Refs. 92 and 96. This study was financed by the Academy of Finland through its Centres of Excellence Program, project no. 251748. N.H. is supported by Aalto University School of Chemical Technology through a PhD scholarship. Computational resources were provided by CSC—the Finnish IT Centre for Science.

Supporting Information Available

The following files are available free of charge. Convergence analysis for the introduced algorithm (Figures S1-S6), additional details regarding the computational methodology, and further numerical results presented in Figures S7-S12 and Tables S1-S6.

Appendix A: Constraint Forces and Atomic Size Adjustments

In this Appendix, we will derive all the necessary relations needed in an MD capable CDFT implementation using the Becke weight, including the necessary modifications to accommodate a heteronuclear charge partitioning. For clarity, we will attempt to keep the notation as close as possible to the original notation of Becke.⁶⁰ To construct the Becke weight function in Equation (9), we define the smoothed step function s as 3rd order iteration of the polynomial p

$$p(\mu_{ij}) = \frac{3}{2}\mu_{ij} - \frac{1}{2}\mu_{ij}^3 \quad (\text{A1})$$

resulting in

$$s(\mu_{ij}) = \frac{1}{2}(1 - f(\mu_{ij})), \quad f(\mu_{ij}) = p\{p[p(\mu_{ij})]\} \quad (\text{A2})$$

With these equations, it is straightforward to incorporate atomic size adjustments into the Becke scheme. In particular, the relevant coordination transformation is defined in terms of μ_{ij} as $\nu_{ij} = \mu_{ij} + a_{ij}(1 - \mu_{ij}^2)$, where the explicit form of a_{ij} is given by

$$a_{ij} = \frac{u_{ij}}{u_{ij}^2 - 1}, \quad u_{ij} = \frac{\chi - 1}{\chi + 1}, \quad \chi = \frac{R_i}{R_j} \quad (\text{A3})$$

and R_i denotes the radius of atom i . Here, a_{ij} is additionally constrained to have values in the range $|a_{ij}| < \frac{1}{2}$ to ensure monotonicity of the coordinate transformation. A heteronuclear charge partitioning is generated by simply substituting μ_{ij} for ν_{ij} in Equation (A1) without the need to modify any of the other expressions.

Next, we proceed onto the calculation of the gradient of the weight function, Equation (11), needed to evaluate the constraint's contribution to the atomic forces. The gradients of the cell functions P_i can be calculated from

$$\begin{aligned}\frac{\partial P_i(\mathbf{r})}{\partial \mathbf{R}_i} &= \sum_{\substack{j \in \mathcal{N} \\ j \neq i}} \frac{P_i(\mathbf{r})}{s(\mu_{ij})} \frac{\partial s(\mu_{ij})}{\partial \mathbf{R}_i} \\ \frac{\partial P_j(\mathbf{r})}{\partial \mathbf{R}_i} &= \frac{P_j(\mathbf{r})}{s(\mu_{ji})} \frac{\partial s(\mu_{ji})}{\partial \mathbf{R}_i}\end{aligned}\tag{A4}$$

In order to evaluate these equations, we first introduce the auxiliary function g and let it denote the gradient of the iterated polynomial p (equation (A1))

$$g(\mu_{ij}) = \frac{\partial p(\mu_{ij})}{\partial \mu_{ij}} = \frac{3}{2} - \frac{3}{2} \mu_{ij}^2\tag{A5}$$

The cell function gradients can now be evaluated using

$$\frac{\partial s(\mu_{ij})}{\partial \mathbf{R}_i} = -\frac{1}{2} \frac{\partial f(\mu_{ij})}{\partial \mu_{ij}} \frac{\partial \mu_{ij}}{\partial \mathbf{R}_i}\tag{A6}$$

where

$$\frac{\partial f(\mu_{ij})}{\partial \mu_{ij}} = \left(\frac{3}{2}\right)^2 g(1-p^2) \left[1 - \left(\frac{3}{2}p - \frac{1}{2}p^3\right)^2\right]\tag{A7}$$

Finally, the required gradients of μ_{ij} are given by

$$\begin{aligned}\frac{\partial \mu_{ij}}{\partial \mathbf{R}_i} &= \frac{\mathbf{r}_i - \mathbf{r}}{|\mathbf{r}_i - \mathbf{r}|} \frac{1}{R_{ij}} - (r_i - r_j) \frac{\mathbf{R}_i - \mathbf{R}_j}{R_{ij}^3} \\ \frac{\partial \mu_{ij}}{\partial \mathbf{R}_j} &= -\left(\frac{\mathbf{r}_j - \mathbf{r}}{|\mathbf{r}_j - \mathbf{r}|} \frac{1}{R_{ij}} - (r_i - r_j) \frac{\mathbf{R}_i - \mathbf{R}_j}{R_{ij}^3}\right)\end{aligned}\tag{A8}$$

In case a heteronuclear partitioning is employed, the gradients of the cell functions need to be modified to account for the change of variables $\mu_{ij} \rightarrow \nu_{ij}$. As explained above, a simple insertion of ν_{ij} in equation (A1) is sufficient to construct the smoothed step function $s(\nu_{ij})$. Hence, the only term that needs more careful attention is the gradient $\partial s(\nu_{ij})/\partial \mathbf{R}_i$. By repeated application of the chain rule, this term can be computed from

$$\begin{aligned}
\frac{\partial s(\nu_{ij})}{\partial \mathbf{R}_i} &= -\frac{1}{2} \frac{\partial f(\nu_{ij})}{\partial \nu_{ij}} \frac{\partial \nu_{ij}}{\partial \mu_{ij}} \frac{\partial \mu_{ij}}{\partial \mathbf{R}_i} \\
&= (1 - 2a_{ij}\mu_{ij}) \left. \frac{\partial s(\mu_{ij})}{\partial \mathbf{R}_i} \right|_{\mu_{ij}=\nu_{ij}}
\end{aligned} \tag{A9}$$

Thus, only a simple multiplication is required to account for heteronuclear partitioning in the constraint force.

Appendix B: Derivation of Symmetry Relations

In the main text, we have shown how using the appropriate symmetry relations can be employed to decrease the computational cost the Becke method. We will now derive these relations. Specifically, the goal is to derive a relationship between $s(\mu_{ij})$ and $s(\mu_{ji})$ (needed to compute the cell function P_j), as well as between their gradients with respect to μ with the same ordering of indices (needed to compute the gradients of P_j with respect to atomic positions \mathbf{R}_i and \mathbf{R}_j). From equation (10), it is clear that $\mu_{ij} = -\mu_{ji}$ since the internuclear separation R_{ij} in the denominator is insensitive to a permutation of the indices. Because the iterated polynomial p , which is used for defining the smoothed step function s , is an odd function, we obtain the following result $f(\mu_{ij}) = -f(\mu_{ji})$. This allows us to determine a relation between the smoothed step functions of atom pairs ij and ji

$$s(\mu_{ji}) = \frac{1}{2} (1 - f(\mu_{ji})) = \frac{1}{2} (1 + f(\mu_{ij})) = s(\mu_{ij}) + f(\mu_{ij}) \tag{B1}$$

This equation facilitates computing the contribution of the atom pair ji to the cell function P_j of atom j while actually iterating over the reverse atom pair ij . To compute the corresponding contribution to the gradients $\partial P_j / \partial \mathbf{R}_i$ and $\partial P_j / \partial \mathbf{R}_j$, we first note that as the gradient of f (equation (A7)) involves only even powers of μ_{ij} , the gradient is symmetric with respect to permuting the indices ij and ji

$$\frac{\partial f(\mu_{ij})}{\partial \mu_{ij}} = \frac{\partial f(\mu_{ji})}{\partial \mu_{ji}} \quad (\text{B2})$$

The above symmetry relations allow us to conclude that

$$\frac{\partial s(\mu_{ij})}{\partial \mu_{ij}} = -\frac{\partial s(\mu_{ji})}{\partial \mu_{ji}} \quad (\text{B3})$$

and so all cell function P_j independent components of the gradient $\partial P_j / \partial \mathbf{R}_i$ can be calculated simultaneously with the construction of the reverse atom pair ij . Since the final value of the cell function P_j is available only after each atom pair has been looped over, any terms involving the gradient $\partial P_j / \partial \mathbf{R}_i$ must be finalized after this value is available. The same considerations apply for the gradient $\partial P_j / \partial \mathbf{R}_j$. For the heteronuclear case, again since $\mu_{ij} = -\mu_{ji}$ and by definition $a_{ij} = -a_{ji}$, the heteronuclear quantity ν_{ij} also satisfies the equation $\nu_{ij} = -\nu_{ji}$. As a result, all of the symmetry relations derived above for the homonuclear case apply directly to heteronuclear partitioning.

References

- (1) Cecchini, G. Function and Structure of Complex II of the Respiratory Chain. *Annu. Rev. Biochem.* **2003**, *72*, 77–109.
- (2) Crofts, A. R. The Cytochrome bc1 Complex: Function in the Context of Structure. *Annu. Rev. of Physiol.* **2004**, *66*, 689–733.
- (3) Sazanov, L. A. A Giant Molecular Proton Pump: Structure and Mechanism of Respiratory Complex I. *Nat. Rev. Mol. Cell Biol.* *16*, 375–388.
- (4) Liu, J.; Chakraborty, S.; Hosseinzadeh, P.; Yu, Y.; Tian, S.; Petrik, I.; Bhagi, A.; Lu, Y. Metalloproteins Containing Cytochrome, Iron–Sulfur, or Copper Redox Centers. *Chem. Rev.* **2014**, *114*, 4366–4469.

- (5) Blumberger, J. Recent Advances in the Theory and Molecular Simulation of Biological Electron Transfer Reactions. *Chem. Rev.* **2015**, *115*, 11191–11238.
- (6) Marcus, R. A. On the Theory of Oxidation-Reduction Reactions Involving Electron Transfer. I. *J. Chem. Phys.* **1956**, *24*, 966–978.
- (7) Newton, M. D.; Sutin, N. Electron Transfer Reactions in Condensed Phases. *Annu. Rev. Phys. Chem.* **1984**, *35*, 437–480.
- (8) Marcus, R.; Sutin, N. Electron Transfers in Chemistry and Biology. *Biochim. Biophys. Acta* **1985**, *811*, 265–322.
- (9) Laborda, E.; Henstridge, M. C.; Batchelor-McAuley, C.; Compton, R. G. Asymmetric Marcus-Hush Theory for Voltammetry. *Chem. Soc. Rev.* **2013**, *42*, 4894–4905.
- (10) Henstridge, M. C.; Laborda, E.; Rees, N. V.; Compton, R. G. Marcus–Hush–Chidsey Theory of Electron Transfer Applied to Voltammetry: A Review. *Electrochim. Acta* **2012**, *84*, 12–20.
- (11) Migliore, A.; Polizzi, N. F.; Therien, M. J.; Beratan, D. N. Biochemistry and Theory of Proton-Coupled Electron Transfer. *Chem. Rev.* **2014**, *114*, 3381–3465.
- (12) Vuilleumier, R.; Tay, K. A.; Jeanmairet, G.; Borgis, D.; Boutin, A. Extension of Marcus Picture for Electron Transfer Reactions with Large Solvation Changes. *J. Am. Chem. Soc.* **2012**, *134*, 2067–2074.
- (13) Troisi, A.; Nitzan, A.; Ratner, M. A. A Rate Constant Expression for Charge Transfer through Fluctuating Bridges. *J. Chem. Phys.* **2003**, *119*, 5782–5788.
- (14) Cave, R. J.; Newton, M. D. Generalization of the Mulliken-Hush Treatment for the Calculation of Electron Transfer Matrix Elements. *Chem. Phys. Lett.* **1996**, *249*, 15–19.

- (15) Cave, R. J.; Newton, M. D. Calculation of Electronic Coupling Matrix Elements for Ground and Excited State Electron Transfer Reactions: Comparison of the Generalized Mulliken–Hush and Block Diagonalization Methods. *J. Chem. Phys.* **1997**, *106*, 9213–9226.
- (16) Subotnik, J. E.; Vura-Weis, J.; Sodt, A. J.; Ratner, M. A. Predicting Accurate Electronic Excitation Transfer Rates via Marcus Theory with Boys or Edmiston–Ruedenberg Localized Diabatization. *J. Phys. Chem. A* **2010**, *114*, 8665–8675.
- (17) Vura-Weis, J.; Newton, M. D.; Wasielewski, M. R.; Subotnik, J. E. Characterizing the Locality of Diabatic States for Electronic Excitation Transfer By Decomposing the Diabatic Coupling. *J. Phys. Chem. C* **2010**, *114*, 20449–20460.
- (18) Fatehi, S.; Alguire, E.; Subotnik, J. E. Derivative Couplings and Analytic Gradients for Diabatic States, with an Implementation for Boys-Localized Configuration-Interaction Singles. *J. Chem. Phys.* **2013**, *139*, 124112.
- (19) Domcke, W.; Woywod, C. Direct Construction of Diabatic States in the CASSCF Approach. Application to the Conical Intersection of the 1A_2 and 1B_1 Excited States of Ozone. *Chem. Phys. Lett.* **1993**, *216*, 362–368.
- (20) Pacher, T.; Cederbaum, L. S.; Köppel, H. Approximately Diabatic States from Block Diagonalization of the Electronic Hamiltonian. *J. Chem. Phys.* **1988**, *89*, 7367–7381.
- (21) Ren, H.; Provorse, M. R.; Bao, P.; Qu, Z.; Gao, J. Multistate Density Functional Theory for Effective Diabatic Electronic Coupling. *J. Phys. Chem. Lett.* **2016**, *7*, 2286–2293.
- (22) Wu, Q.; Van Voorhis, T. Extracting Electron Transfer Coupling Elements from Constrained Density Functional Theory. *J. Chem. Phys.* **2006**, *125*, 164105.

- (23) Oberhofer, H.; Blumberger, J. Electronic Coupling Matrix Elements from Charge Constrained Density Functional Theory Calculations Using a Plane Wave Basis Set. *J. Chem. Phys.* **2010**, *133*, 244105.
- (24) de la Lande, A.; Salahub, D. R. Derivation of Interpretative Models for Long Range Electron Transfer from Constrained Density Functional Theory. *J. Mol. Struct. Theochem* **2010**, *943*, 115–120.
- (25) Subotnik, J. E.; Yeganeh, S.; Cave, R. J.; Ratner, M. A. Constructing Diabatic States from Adiabatic States: Extending Generalized Mulliken–Hush to Multiple Charge Centers with Boys Localization. *J. Chem. Phys.* **2008**, *129*, 244101.
- (26) Subotnik, J. E.; Cave, R. J.; Steele, R. P.; Shenvi, N. The Initial and Final States of Electron and Energy Transfer Processes: Diabatization as Motivated by System-Solvent Interactions. *J. Chem. Phys.* **2009**, *130*, 234102.
- (27) Migliore, A. Nonorthogonality Problem and Effective Electronic Coupling Calculation: Application to Charge Transfer in π -Stacks Relevant to Biochemistry and Molecular Electronics. *J. Chem. Theory Comput.* **2011**, *7*, 1712–1725.
- (28) Ramos, P.; Mankarious, M.; Pavanello, M. In *Practical Aspects of Computational Chemistry IV*; Leszczynski, J., Shukla, M. K., Eds.; Springer US: Boston, MA, 2016; pp 103–134.
- (29) Coropceanu, V.; Cornil, J.; da Silva Filho, D. A.; Olivier, Y.; Silbey, R.; Brédas, J.-L. Charge Transport in Organic Semiconductors. *Chem. Rev.* **2007**, *107*, 926–952.
- (30) Kaduk, B.; Kowalczyk, T.; Voorhis, T. V. Constrained Density Functional Theory. *Chem. Rev.* **2012**, *112*, 321–370.
- (31) Stuchebrukhov, A. A. Long-Distance Electron Tunneling in Proteins. *Theor. Chem. Acc.* **2003**, *110*, 291–306.

- (32) Hsu, C.-P. The Electronic Couplings in Electron Transfer and Excitation Energy Transfer. *Acc. Chem. Res.* **2009**, *42*, 509–518.
- (33) Kawatsu, T. Review Pathway Analysis for Peptide-Mediated Electronic Coupling in the Super-Exchange Mechanism of ET and EET. *Pept. Sci.* **2013**, *100*, 100–113.
- (34) Mavros, M. G.; Van Voorhis, T. Communication: CDFT-CI Couplings Can Be Unreliable when There Is Fractional Charge Transfer. *J. Chem. Phys.* **2015**, *143*, 231102.
- (35) Mori-Sánchez, P.; Cohen, A. J.; Yang, W. Many-Electron Self-Interaction Error in Approximate Density Functionals. *J. Chem. Phys.* **2006**, *125*, 201102.
- (36) Parthey, M.; Kaupp, M. Quantum-Chemical Insights into Mixed-Valence Systems: Within and Beyond the Robin-Day Scheme. *Chem. Soc. Rev.* **2014**, *43*, 5067–5088.
- (37) Oberhofer, H.; Blumberger, J. Charge Constrained Density Functional Molecular Dynamics for Simulation of Condensed Phase Electron Transfer Reactions. *J. Chem. Phys.* **2009**, *131*, 064101.
- (38) Oberhofer, H.; Blumberger, J. Insight into the Mechanism of the Ru²⁺-Ru³⁺ Electron Self-Exchange Reaction from Quantitative Rate Calculations. *Angew. Chem. Int. Ed.* **2010**, *49*, 3631–3634.
- (39) Kowalczyk, T.; Wang, L.-P.; Van Voorhis, T. Simulation of Solution Phase Electron Transfer in a Compact Donor-Acceptor Dyad. *J. Phys. Chem. B* **2011**, *115*, 12135–12144.
- (40) Řezáč, J.; Lévy, B.; Demachy, I.; de la Lande, A. Robust and Efficient Constrained DFT Molecular Dynamics Approach for Biochemical Modeling. *J. Chem. Theory Comput.* **2012**, *8*, 418–427.
- (41) Firmino, T.; Mangaud, E.; Cailliez, F.; Devolder, A.; Mendive-Tapia, D.; Gatti, F.; Meier, C.; Desouter-Lecomte, M.; de la Lande, A. Quantum Effects in Ultrafast Elec-

- tron Transfers within Cryptochromes. *Phys. Chem. Chem. Phys.* **2016**, *18*, 21442–21457.
- (42) Wu, Q.; Van Voorhis, T. Direct Optimization Method to Study Constrained Systems within Density-Functional Theory. *Phys. Rev. A* **2005**, *72*, 024502.
- (43) Wu, Q.; Van Voorhis, T. Direct Calculation of Electron Transfer Parameters through Constrained Density Functional Theory. *J. Phys. Chem. A* **2006**, *110*, 9212–9218.
- (44) Sena, A. M. P.; Miyazaki, T.; Bowler, D. R. Linear Scaling Constrained Density Functional Theory in CONQUEST. *J. Chem. Theory Comput.* **2011**, *7*, 884–889.
- (45) Shao, Y.; Gan, Z.; Epifanovsky, E.; Gilbert, A. T.; Wormit, M.; Kussmann, J.; Lange, A. W.; Behn, A.; Deng, J.; Feng, X. et al. Advances in Molecular Quantum Chemistry Contained in the Q-Chem 4 Program Package. *Mol. Phys.* **2015**, *113*, 184–215.
- (46) Souza, A. M.; Rungger, I.; Pemmaraju, C. D.; Schwingenschloegl, U.; Sanvito, S. Constrained-DFT Method for Accurate Energy-Level Alignment of Metal/Molecule Interfaces. *Phys. Rev. B* **2013**, *88*, 165112.
- (47) Ratcliff, L. E.; Genovese, L.; Mohr, S.; Deutsch, T. Fragment Approach to Constrained Density Functional Theory Calculations Using Daubechies Wavelets. *J. Chem. Phys.* **2015**, *142*, 234105.
- (48) VandeVondele, J.; Hutter, J. An Efficient Orbital Transformation Method for Electronic Structure Calculations. *J. Chem. Phys.* **2003**, *118*, 4365–4369.
- (49) Lippert, G.; Hutter, J.; Parrinello, M. A Hybrid Gaussian and Plane Wave Density Functional Scheme. *Mol. Phys.* **1997**, *92*, 477–488.
- (50) VandeVondele, J.; Krack, M.; Mohamed, F.; Parrinello, M.; Chassaing, T.; Hutter, J.

- Quickstep: Fast and Accurate Density Functional Calculations Using a Mixed Gaussian and Plane Waves Approach. *Comput. Phys. Commun.* **2005**, *167*, 103–128.
- (51) Hutter, J.; Iannuzzi, M.; Schiffmann, F.; VandeVondele, J. CP2K: Atomistic Simulations of Condensed Matter Systems. *Wiley Interdiscip. Rev.: Comput. Mol. Sci.* **2014**, *4*, 15–25.
- (52) Tocci, G.; Joly, L.; Michaelides, A. Friction of Water on Graphene and Hexagonal Boron Nitride from Ab Initio Methods: Very Different Slippage Despite Very Similar Interface Structures. *Nano Lett.* **2014**, *14*, 6872–6877.
- (53) Ding, Y.; Hassanali, A. A.; Parrinello, M. Anomalous Water Diffusion in Salt Solutions. *Proc. Natl. Acad. Sci. USA* **2014**, *111*, 3310–3315.
- (54) Mason, P. E.; Uhlig, F.; Vaněk, V.; Buttersack, T.; Bauerecker, S.; Jungwirth, P. Coulomb Explosion during the Early Stages of the Reaction of Alkali Metals with Water. *Nat. Chem.* **2015**, *7*, 250–254.
- (55) Dederichs, P. H.; Blügel, S.; Zeller, R.; Akai, H. Ground States of Constrained Systems: Application to Cerium Impurities. *Phys. Rev. Lett.* **1984**, *53*, 2512–2515.
- (56) Wu, Q.; ; Voorhis, T. V. Constrained Density Functional Theory and Its Application in Long-Range Electron Transfer. *J. Chem. Theory Comput.* **2006**, *2*, 765–774.
- (57) Wu, Q.; Cheng, C.-L.; Van Voorhis, T. Configuration Interaction Based on Constrained Density Functional Theory: A Multireference Method. *J. Chem. Phys.* **2007**, *127*, 164119.
- (58) Wu, Q.; Kaduk, B.; Van Voorhis, T. Constrained Density Functional Theory Based Configuration Interaction Improves the Prediction of Reaction Barrier Heights. *J. Chem. Phys.* **2009**, *130*, 034109.

- (59) Hirshfeld, F. L. Bonded-Atom Fragments for Describing Molecular Charge Densities. *Theoret. Chim. Acta* **1977**, *44*, 129–138.
- (60) Becke, A. D. A Multicenter Numerical Integration Scheme for Polyatomic Molecules. *J. Chem. Phys.* **1988**, *88*, 2547–2553.
- (61) Warshel, A. Dynamics of Reactions in Polar Solvents. Semiclassical Trajectory Studies of Electron-Transfer and Proton-Transfer Reactions. *J. Phys. Chem.* **1982**, *86*, 2218–2224.
- (62) Weber, V.; VandeVondele, J.; Hutter, J.; Niklasson, A. M. N. Direct Energy Functional Minimization under Orthogonality Constraints. *J. Chem. Phys.* **2008**, *128*, 084113.
- (63) Kolafa, J. Time-Reversible Always Stable Predictor–Corrector Method for Molecular Dynamics of Polarizable Molecules. *J. Comput. Chem.* **2004**, *25*, 335–342.
- (64) Lippert, G.; Hutter, J.; Parrinello, M. The Gaussian and Augmented-Plane-Wave Density Functional Method for Ab Initio Molecular Dynamics Simulations. *Theor. Chem. Acc.* **1999**, *103*, 124–140.
- (65) VandeVondele, J.; Hutter, J. Gaussian Basis Sets for Accurate Calculations on Molecular Systems in Gas and Condensed Phases. *J. Chem. Phys.* **2007**, *127*, 114105.
- (66) Goedecker, S.; Teter, M.; Hutter, J. Separable Dual-Space Gaussian Pseudopotentials. *Phys. Rev. B* **1996**, *54*, 1703–1710.
- (67) Hartwigsen, C.; Goedecker, S.; Hutter, J. Relativistic Separable Dual-Space Gaussian Pseudopotentials from H to Rn. *Phys. Rev. B* **1998**, *58*, 3641–3662.
- (68) Krack, M. Pseudopotentials for H to Kr Optimized for Gradient-Corrected Exchange-Correlation Functionals. *Theor. Chem. Acc.* **2005**, *114*, 145–152.

- (69) Marek, A.; Blum, V.; Johanni, R.; Havu, V.; Lang, B.; Auckenthaler, T.; Heinecke, A.; Bungartz, H.-J.; Lederer, H. The ELPA Library: Scalable Parallel Eigenvalue Solutions for Electronic Structure Theory and Computational Science. *J. Phys. Condens. Matter* **2014**, *26*, 213201.
- (70) Grimme, S.; Antony, J.; Ehrlich, S.; Krieg, H. A Consistent and Accurate Ab Initio Parametrization of Density Functional Dispersion Correction (DFT-D) for the 94 Elements H-Pu. *J. Chem. Phys.* **2010**, *132*, 154104.
- (71) Grimme, S.; Ehrlich, S.; Goerigk, L. Effect of the Damping Function in Dispersion Corrected Density Functional Theory. *J. Comput. Chem.* **2011**, *32*, 1456–1465.
- (72) Perdew, J. P.; Burke, K.; Ernzerhof, M. Generalized Gradient Approximation Made Simple. *Phys. Rev. Lett.* **1996**, *77*, 3865–3868.
- (73) Adamo, C.; Barone, V. Toward Reliable Density Functional Methods without Adjustable Parameters: The PBE0 Model. *J. Chem. Phys.* **1999**, *110*, 6158–6170.
- (74) Becke, A. D. Density-Functional Exchange-Energy Approximation with Correct Asymptotic Behavior. *Phys. Rev. A* **1988**, *38*, 3098–3100.
- (75) Lee, C.; Yang, W.; Parr, R. G. Development of the Colle-Salvetti Correlation-Energy Formula into a Functional of the Electron Density. *Phys. Rev. B* **1988**, *37*, 785–789.
- (76) Stephens, P. J.; Devlin, F. J.; Chabalowski, C. F.; Frisch, M. J. Ab Initio Calculation of Vibrational Absorption and Circular Dichroism Spectra Using Density Functional Force Fields. *J. Phys. Chem.* **1994**, *98*, 11623–11627.
- (77) Guidon, M.; Hutter, J.; Vandevondele, J. Robust Periodic Hartree-Fock Exchange for Large-Scale Simulations Using Gaussian Basis Sets. *J. Chem. Theory Comput.* **2009**, *5*, 3010–3021.

- (78) Guidon, M.; Hutter, J.; VandeVondele, J. Auxiliary Density Matrix Methods for Hartree-Fock Exchange Calculations. *J. Chem. Theory Comput.* **2010**, *6*, 2348–2364.
- (79) Martyna, G. J.; Tuckerman, M. E. A Reciprocal Space Based Method for Treating Long Range Interactions in Ab Initio and Force-Field-Based Calculations in Clusters. *J. Chem. Phys.* **1999**, *110*, 2810–2821.
- (80) Bussi, G.; Donadio, D.; Parrinello, M. Canonical Sampling through Velocity Rescaling. *J. Chem. Phys.* **2007**, *126*, 014101.
- (81) Laino, T.; Mohamed, F.; Laio, A.; Parrinello, M. An Efficient Real Space Multigrid QM/MM Electrostatic Coupling. *J. Chem. Theory Comput.* **2005**, *1*, 1176–1184.
- (82) Laino, T.; Mohamed, F.; Laio, A.; Parrinello, M. An Efficient Linear-Scaling Electrostatic Coupling for Treating Periodic Boundary Conditions in QM/MM Simulations. *J. Chem. Theory Comput.* **2006**, *2*, 1370–1378.
- (83) Pyykkö, P.; Atsumi, M. Molecular Single-Bond Covalent Radii for Elements 1–118. *Chem. Eur. J.* **2009**, *15*, 186–197.
- (84) Pyykkö, P.; Atsumi, M. Molecular Double-Bond Covalent Radii for Elements Li–E112. *Chem. Eur. J.* **2009**, *15*, 12770–12779.
- (85) Shannon, R. D. Revised Effective Ionic Radii and Systematic Studies of Interatomic Distances in Halides and Chalcogenides. *Acta Crystallogr. Sect. A* **1976**, *32*, 751–767.
- (86) Pershin, A.; Szalay, P. G. Development of Highly Accurate Approximate Scheme for Computing the Charge Transfer Integral. *J. Chem. Phys.* **2015**, *143*, 074109.
- (87) Weigend, F.; Ahlrichs, R. Balanced Basis Sets of Split Valence, Triple Zeta Valence and Quadruple Zeta Valence Quality for H to Rn: Design and Assessment of Accuracy. *Phys. Chem. Chem. Phys.* **2005**, *7*, 3297–3305.

- (88) Pieniazek, P. A.; Arnstein, S. A.; Bradforth, S. E.; Krylov, A. I.; Sherrill, C. D. Benchmark Full Configuration Interaction and Equation-of-Motion Coupled-Cluster Model with Single and Double substitutions for Ionized Systems Results for Prototypical Charge Transfer Systems: Noncovalent Ionized Dimers. *J. Chem. Phys.* **2007**, *127*, 164110.
- (89) Kubas, A.; Hoffmann, F.; Heck, A.; Oberhofer, H.; Elstner, M.; Blumberger, J. Electronic Couplings for Molecular Charge Transfer: Benchmarking CDFT, FODFT, and FODFTB against High-Level Ab Initio Calculations. *J. Chem. Phys.* **2014**, *140*, 104105.
- (90) Kubas, A.; Gajdos, F.; Heck, A.; Oberhofer, H.; Elstner, M.; Blumberger, J. Electronic Couplings for Molecular Charge Transfer: Benchmarking CDFT, FODFT and FODFTB against High-Level Ab Initio Calculations. II. *Phys. Chem. Chem. Phys.* **2015**, *17*, 14342–14354.
- (91) Pershin, A.; Szalay, P. G. Improving the Accuracy of the Charge Transfer Integrals Obtained by Coupled Cluster Theory, MBPT(2), and TDDFT. *J. Chem. Theory Comput.* **2015**, *11*, 5705–5711.
- (92) Řezáč, J.; de la Lande, A. Robust, Basis-Set Independent Method for the Evaluation of Charge-Transfer Energy in Noncovalent Complexes. *J. Chem. Theory Comput.* **2015**, *11*, 528–537.
- (93) Řezáč, J.; de la Lande, A. On the Role of Charge Transfer in Halogen Bonding. *Phys. Chem. Chem. Phys. Advance Article*, DOI: 10.1039/C6CP07475H.
- (94) Lao, K. U.; Herbert, J. M. Energy Decomposition Analysis with a Stable Charge-Transfer Term for Interpreting Intermolecular Interactions. *J. Chem. Theory Comput.* **2016**, *12*, 2569–2582.

- (95) Phipps, M. J. S.; Fox, T.; Tautermann, C. S.; Skylaris, C.-K. Energy Decomposition Analysis Approaches and Their Evaluation on Prototypical Protein-Drug Interaction Patterns. *Chem. Soc. Rev.* **2015**, *44*, 3177–3211.
- (96) Karthikeyan, S.; Sedlak, R.; Hobza, P. On the Nature of Stabilization in Weak, Medium, and Strong Charge-Transfer Complexes: CCSD(T)/CBS and SAPT Calculations. *J. Phys. Chem. A* **2011**, *115*, 9422–9428.
- (97) Řezáč, J.; Riley, K. E.; Hobza, P. S66: A Well-Balanced Database of Benchmark Interaction Energies Relevant to Biomolecular Structures. *J. Chem. Theory Comput.* **2011**, *7*, 2427–2438.
- (98) Robin, M. B.; Day, P. In *Mixed Valence Chemistry—A Survey and Classification*; Emeléus, H., Sharpe, A., Eds.; Advances in Inorganic Chemistry and Radiochemistry; Academic Press, 1968; Vol. 10; pp 247–422.
- (99) Gautier, N.; Dumur, F.; Lloveras, V.; Vidal-Gancedo, J.; Veciana, J.; Rovira, C.; Hudhomme, P. Intramolecular Electron Transfer Mediated by a Tetrathiafulvalene Bridge in a Purely Organic Mixed-Valence System. *Angew. Chem. Int. Ed.* **2003**, *42*, 2765–2768.
- (100) Calbo, J.; Aragó, J.; Ortí, E. Theoretical Study of the Benzoquinone–Tetrathiafulvalene–Benzoquinone Triad in Neutral and Oxidized/Reduced States. *Theor. Chem. Acc.* **2013**, *132*, 1–10.
- (101) Vydrov, O. A.; Scuseria, G. E. Assessment of a Long-Range Corrected Hybrid Functional. *J. Chem. Phys.* **2006**, *125*, 234109.
- (102) Renz, M.; Kaupp, M. Predicting the Localized/Delocalized Character of Mixed-Valence Diquinone Radical Anions. Toward the Right Answer for the Right Reason. *J. Phys. Chem. A* **2012**, *116*, 10629–10637.

- (103) Kalinowski, J.; Berski, S.; Gordon, A. J. Electron Localization Function Study on Intramolecular Electron Transfer in the QTTFQ and DBTTFI Radical Anions. *J. Phys. Chem. A* **2011**, *115*, 13513–13522.
- (104) Renz, M.; Theilacker, K.; Lambert, C.; Kaupp, M. A Reliable Quantum-Chemical Protocol for the Characterization of Organic Mixed-Valence Compounds. *J. Am. Chem. Soc.* **2009**, *131*, 16292–16302.
- (105) Kaupp, M.; Renz, M.; Parthey, M.; Stolte, M.; Wurthner, F.; Lambert, C. Computational and Spectroscopic Studies of Organic Mixed-Valence Compounds: Where Is the Charge? *Phys. Chem. Chem. Phys.* **2011**, *13*, 16973–16986.
- (106) Renz, M.; Kess, M.; Diedenhofen, M.; Klamt, A.; Kaupp, M. Reliable Quantum Chemical Prediction of the Localized/Delocalized Character of Organic Mixed-Valence Radical Anions. From Continuum Solvent Models to Direct-COSMO-RS. *J. Chem. Theory Comput.* **2012**, *8*, 4189–4203.

Graphical TOC Entry

Electron transfer parameters

